

1 **Late Eocene to early Oligocene productivity events in the proto-** 2 **Southern Ocean and correlation to climate change**

3 Gabrielle Rodrigues de Faria^{1, 2}, David Lazarus¹, Johan Renaudie¹, Jessica Stammeier³, Volkan
4 Özen^{1,2}, Ulrich Struck^{1,2}

5 ¹Museum für Naturkunde, Leibniz Institute for Evolution and Biodiversity Science, Invalidenstraße, 43, Berlin, 10115,
6 Germany

7 ²Freie Universität Berlin, Institute for Geological Sciences, Malteserstraße 74-100, Berlin, 12249, Germany

8 ³GFZ German Research Centre for Geosciences, Telegrafenberg, Potsdam, 14473, Germany

9 *Correspondence to:* Gabrielle Rodrigues de Faria (gabrielle.faria@mfh.berlin)

10 **Abstract.** The Eocene-Oligocene transition (EOT, ca 40-33 Ma) marks a transformation from a largely ice-free to an
11 ice-house climate mode that is well recorded by oxygen stable isotopes and sea surface temperature proxies. Opening of
12 the Southern Ocean gateways and decline in atmospheric carbon dioxide levels have been considered as factors in this
13 global environmental transformation and the growth of ice sheets in Antarctica during the Cenozoic. A more
14 comprehensive understanding is still needed of the interplay between forcing versus response, the correlation among
15 environmental changes and the involved feedback mechanisms. In this study, we investigate the spatio-temporal
16 variation in export productivity using biogenic Ba (bio-Ba) from Ocean Drilling Program (ODP) Sites in the Southern
17 Ocean, focusing on possible mechanisms that controlled them as well as the correlation of export productivity changes
18 to changes in the global carbon cycle. We document two high export productivity events in the Southern Ocean during
19 the late-Eocene (ca. 37 and 33.5 Ma) that correlate to proposed gateway-driven changes in regional circulation, and to
20 changes in global atmospheric $p\text{CO}_2$ levels. Our findings suggest that paleoceanographic changes following Southern
21 Ocean gateway openings, along with more variable increases in circulation driven by episodic Antarctica ice sheet
22 expansion, enhanced export production in the Southern Ocean from the late Eocene through basal Oligocene. These
23 factors may have played a role in episodic atmospheric carbon dioxide reduction, contributing to Antarctic glaciation
24 during the Eocene-Oligocene transition.

25 **1 Introduction**

26 **1.1 Late Eocene Events as Precursor to Antarctic Eocene/Oligocene Boundary Glaciation**

27 The Eocene-Oligocene transition (EOT, ~ 40-33 Ma) is the most important climatic interval of the Cenozoic era
28 (Westerhold et al., 2020). This interval involves profound transformations in environmental conditions including the
29 onset of continental-scale Antarctica glaciation at the Eocene-Oligocene boundary (Shackleton & Kennett, 1975,
30 Zachos et al., 1996, Coxall et al., 2005), sea-level fall (Houben et al., 2012) and global cooling (Prothero and Berggren,
31 1992; Liu et al., 2009; Bohaty et al., 2012; Hutchinson et al., 2021) as evidenced by a global shift in oxygen isotope
32 records from biogenic calcium carbonate (>1‰; Zachos et al. 2001; Coxall et al. 2005; Bohaty et al., 2012; Westerhold
33 et al., 2020). A positive deep-sea carbon isotope excursion of up to 1‰ (Zachos et al., 2001, Coxall et al., 2005; Coxall
34 and Wilson, 2011; Westerhold et al., 2020) and a change from a shallow (~3.5 km) to a deeper (~4.5 km) calcite
35 compensation depth (CCD) (Coxall et al., 2005; Rea and Lyle, 2005; Pälike et al., 2012; Dutkiewicz and Müller, 2021;

36 Taylor et al., 2023) have also been observed and indicate that the carbon cycle played an important role in the changes
37 observed during the transition, although the mechanisms that caused the carbon cycle perturbation are still unsolved.
38 Carbon cycling acts through a variety of feedback mechanisms. Even though it is well recognized that changes in
39 atmospheric carbon dioxide (CO₂) impact the Earth's climate because of its large effect on temperature (Arrhenius,
40 1896; IPCC, 2021), the mechanisms controlling CO₂ levels over long timescales are still a matter of debate. A
41 simplified carbon cycle theory suggests that the level of CO₂ is expected to remain in a steady state over multi
42 millennial (>10 kyr) timescales (Berner et al., 1983; DeVries, 2022). This stability is attributed to a dynamic interplay
43 of transfer of carbon between volcanic inputs, oceans, atmosphere and sequestration in marine sediments involving
44 several mechanisms such as weathering, volcanism, and the ocean's biological pump.
45 However, the Earth's *p*CO₂ has, in fact, undergone substantial changes, from Glacial-Interglacial timescales (Sigman &
46 Boyle, 2000) to long term changes during the Cenozoic (Beerling and Royer, 2011; Anagnostou et al., 2016), thus
47 suggesting that the Earth's carbon system operates in a more complex way than proposed in the canonical model.
48 Changes in the Southern Ocean productivity are thought to have altered *p*CO₂ levels in the Earth's past, specifically on
49 Glacial-Interglacial timescales (Archer et al., 2000; Sigman et al., 2010), although magnitude and timing remain
50 debated. Changes in the late-Eocene Southern Ocean export productivity over 1 million years, as documented in our
51 research, could potentially have impacted CO₂ levels, as hypothesized by Egan et al., (2013), based on Si isotope proxy
52 data for Paleogene Southern Ocean diatom productivity.

53 The carbon cycle perturbation at the EOT provides an opportunity to understand climate-carbon cycle feedback (Zachos
54 and Kump, 2005). The mechanisms proposed to explain such perturbations are processes operating gradually over long
55 timescales, and may have had their origins in the middle to late Eocene. Preceding the abrupt change at the E/O
56 boundary, the late Eocene was a period of gradual cooling and progressive CO₂ levels decrease (Lauretano et al., 2021).
57 The events associated with this time period may have had substantial importance in pre-conditioning the climate system
58 prior to the major climatic shift at the E/O boundary (Egan et al., 2013). The potential main drivers for the initiation of
59 this global cooling and ice build-up in Antarctica are actively debated. Declining global atmospheric carbon dioxide
60 concentrations, and the opening of Southern Hemisphere oceanic gateways, namely the Drake Passage (DP) and the
61 Tasmanian Gateway (TG), are often proposed hypotheses to explain this transition (Coxall and Pearson, 2007; DeConto
62 et al. 2008). The decline of carbon dioxide levels is an important factor in driving cooler temperatures, and has been
63 suggested as the crucial factor in the EOT cooling and subsequent build-up of continental glaciers on Antarctica
64 (DeConto and Pollard, 2003; Huber and Nof, 2006; Pagani et al., 2011). Atmospheric CO₂ partial pressure (*p*CO₂)
65 decline has robust observational support. Atmospheric *p*CO₂ has been shown to decline through the Eocene, from ca
66 1400 p.p.m. at the Early Eocene Climate Optimum (EECO, ca 51 to 53 million years ago) to about 770 p.p.m. in the
67 late-Eocene, reaching a minimum of 550 ± 190 p.p.m. in the early Oligocene (Anagnostou et al. 2016). However, data is
68 noisy, with significant variations among different proxies and thus details of the magnitude and timing are still unclear.
69 Furthermore, the CO₂ threshold (~ 780 p.p.m.v) needed for the onset of Antarctica glaciation, is highly dependent on
70 model boundary conditions while ice sheet model simulations reveal inter-model disagreement (Gasson et al., 2014).
71 Therefore, it is crucial to approach this leading hypothesis with caution due to these uncertainties.

72 The tectonic opening of the Southern Ocean gateways is considered a mechanism contributing to the climatic shift
73 because it allows the initiation of a circum-Antarctic flow, leading to the formation of the Antarctic Circumpolar
74 Current (ACC) (Kennett, 1977; Barker, 2001; Scher and Martin, 2006; Toumoulin et al. 2020). This intense eastward
75 flowing current is proposed in this hypothesis to impact the regional and global climate by preventing tropical heat of

76 low latitudes from reaching Antarctica, promoting the thermal isolation of Antarctica. Numerous ocean circulation
77 model studies of this hypothesis have yielded conflicting results (Mikolajewicz et al., 1993; Najjar et al., 2002; De
78 Conto & Pollard, 2003; Sijp et al., 2009; Goldner et al., 2014; Ladant et al., 2014; Inglis et al., 2015) but most of these
79 earlier works were limited by unrealistic boundary conditions or other issues (Toumoulin et al., 2020, Hutchinson et al.,
80 2021). Recent modelling circulation studies (e.g. Toumoulin et al., 2020; Sauermilch, et al. 2021) demonstrate the
81 importance of the Southern gateway openings and the proto-ACC on ocean cooling in the Southern Hemisphere.
82 Additionally, glaciation has itself a strong influence both on the circulation of the Southern Ocean and on global
83 climate, via increased albedo, colder temperatures and increased latitudinal temperature gradients, and stronger zonal
84 winds (Goldner et al., 2014). There is increasing evidence for at least partial, if transient Antarctic continental glaciation
85 within the late Eocene (Scher and Martin, 2014), and thus this also needs to be considered in understanding how climate
86 and ocean change developed within this period.

87 In addition to the above physical impacts, the ACC is associated with the development of the Southern Ocean fronts that
88 contribute to upwelling-induced biological productivity (Chapman et al., 2020). Considering that the changes in the
89 Southern Ocean circulation have the potential to affect export productivity and via its link to carbon sequestration in
90 sediments, in removing CO₂ from the ocean-atmosphere system, the 'CO₂' hypothesis and the 'tectonic' hypothesis may
91 be linked, via the influence that gateways may have had on Southern Ocean circulation, increasing export productivity
92 enough to affect global *p*CO₂ (Egan et al., 2013). Therefore, evaluating export productivity patterns in the Southern
93 Ocean across the Eocene-Oligocene and its relationship with circulation and decline of atmospheric carbon dioxide
94 during this time period provide important information about possible climate feedbacks in this prominent climatic
95 transition.

96 Many studies have shown variations in biological productivity during this time interval (Diester-Haass, 1995; Diester-
97 Haass and Zahn, 1996; 2001, Salamy and Zachos, 1999; Diester-Haass and Zachos, 2003; Schumacher and Lazarus,
98 2004; Anderson and Delaney, 2005; Villa et al., 2014), pointing towards a productivity increase associated with ocean
99 circulation changes that increased surface water nutrient availability (Diester-Haass 1992; Zachos et al 1996). However,
100 existing studies have mostly focused on single sites, whose paleoceanographic history may reflect local rather than
101 regional developments. A much broader spatial investigation is particularly important for understanding the influence of
102 large-scale ocean circulation on this process. Moreover, the timing of productivity changes differs among the studies
103 and different proxies, limiting our understanding of cause-and-effect relationship. This highlights the importance of well
104 constrained age models and use of consistent paleoproductivity proxies.

105 Here, we reconstruct changes in export productivity in the Southern Ocean across the late Eocene and early Oligocene,
106 and evaluate how the changes observed may be linked to ocean circulation changes and how they may have contributed
107 to the climate changes observed at this interval. We utilize biogenic barium (bio-Ba) accumulation rates to measure
108 marine export productivity. Bio-Ba is defined as the fraction of total barium that is not associated with terrigenous
109 sources, sometimes referred to as *excess*-Ba (Dymond et al., 1992), and has been applied in several studies in the
110 Paleogene (eg. Nielsen et al., 2003; Anderson and Delaney, 2005; Faul and Delaney, 2010). It is considered a relatively
111 reliable proxy to estimate changes in paleoproductivity in the Southern Ocean. Newly generated carbon and oxygen
112 stable isotope records from the same samples of our bio-Ba data further constrain possible causative mechanisms for the
113 climatic shift at the EOT. We compare our export productivity proxy results to indicators of ocean circulation change,
114 such as Neodymium (Nd) isotopes. Neodymium isotopes have emerged as a valuable geochemical water mass tracer
115 (Piepgras and Wasserburg, 1982; Martin and Haley, 2000, Roberts et al., 2010), contributing significantly to our

116 understanding of the role of ocean circulation in the geological past. This proxy provides an opportunity to assess the
117 origin of water masses and reconstruct deep ocean circulation. Here, we use Nd isotope data to help understand gateway
118 opening, paleoceanographic changes and ice sheet history during the Eocene-Oligocene transition, and how these
119 changes may have influenced marine biological productivity. We also compare our productivity records to well
120 established proxies for the global carbon cycle, specifically $p\text{CO}_2$ and $\delta^{13}\text{C}$ of benthic deep sea foraminifera.
121 Our understanding of the Eocene-Oligocene transition has been enhanced through modelling studies as they provide
122 means to compare several possible scenarios and generate ‘data’ for components of the system for which no direct
123 proxy data is available. However, all models are simplifications of complex, not fully understood systems; and are
124 dependent on parametrizations and calibrations to often sparse, noisy proxies that ground-truth model outputs. This
125 paper instead focuses on proxy evidence of the changes that occurred in this time interval.

126 **1.2. Paleooceanographic Setting**

127 The Southern Ocean (SO) today is an important part of the global ocean circulation and climate system, interconnecting
128 the Atlantic, Pacific and Indian Ocean basins, providing and thus inter-basin exchange of ocean properties and heat
129 (Rintoul et al., 2001). There are strong latitudinal gradients and seasonal changes in ocean properties which affect
130 surface water and export productivity, and thus this region’s role in global carbon capture and sequestration. Low light
131 levels and, in higher latitudes, extensive sea ice limit productivity during the winter months. Deep surface mixed layers
132 over the large areas of the Southern Ocean, beyond the shallow stratification effects of meltwater near the sea ice edge,
133 also tend to limit productivity in spring through fall as plankton is mixed below critical thresholds of light availability
134 (Deppeler and Davidson, 2017). The relationship between mixed layer thickness and productivity however is complex
135 (Nelson and Smith, 1991; Li et al. 2021). Southern Ocean productivity is thus concentrated near the Antarctic
136 Circumpolar Current (ACC), the dominant current in the region. This current is the longest and strongest ocean current
137 on Earth. This complex circulation system is driven mainly by westerly winds, resulting in Ekman transport and
138 favouring deep water upwelling. This flow pattern is possible in the absence of land barriers and is governed by
139 bathymetry (Rintoul et al., 2001; Carter et al., 2008), while the strength of the current is driven by the strength and
140 location of the westerly winds, and thus, among other factors, the global latitudinal thermal gradient. The ACC is a key
141 component of the ‘ocean conveyor belt’, playing a role in the global transport of heat (Rintoul et al., 2001; Katz, et al.
142 2011). Moreover, this circumpolar current influences the strength of meridional overturning circulation and several
143 authors have proposed that this current is one of the main drivers of the Atlantic meridional overturning circulation
144 (AMOC) (Toggweiler and Samuels, 1995; Toggweiler and Bjornsson, 2000; Scher and Martin, 2006, Kuhlbrodt et al.,
145 2007, Scher et al., 2015, Sarkar et al., 2019).

146 The ACC is structured of multiple hydrological fronts, associated with specific water mass properties such as
147 temperature and salinity (Sokolov and Rintoul, 2009). Orsi et al., 1995 proposed the traditional view of Southern Ocean
148 fronts. It consists of the Subantarctic Front (SAF), the Antarctic Polar Front (APF) and the Southern ACC Front
149 (SACCF). Besides these main fronts, a Subtropical Frontal Zone (STFZ) can be found north of the ACC (Orsi et al.,
150 1995; Palter et al. 2013; Chapman et al., 2020). This frontal structure is fundamental to different processes that occur in
151 the region, such as the distribution of important nutrients through the exchange between deep and surface ocean, and the
152 exchange of tracers (Palter et al., 2013). Upwelling of Circumpolar Deep Water (CDW) brings nutrient-rich waters to
153 the surface towards the Polar Front Zone (PFZ) where Antarctic Surface Waters (AASW) sink to form Antarctic
154 Intermediate Water (AAIW), thereafter it extends into the Subantarctic Zone (SAZ) (Sarmiento et al., 2004) (Figure 1).

155 Wind-driven upwelling, that occurs within the Southern Ocean fronts, enhances biological productivity in these regions
156 (De Baar et al., 1995; Moore et al., 1999). More recently, upwelling related to ACC bathymetry has been found as an
157 important mechanism for establishing phytoplankton blooms in the SO (Sokolov and Rintoul, 2007). This complex
158 structure involving ACC fronts, westerlies and the bottom topography, makes the Southern Ocean a highly productive
159 region. Iron remobilisation has also been shown to occur due to latitudinal variations of the ACC (Kim et al., 2009),
160 inducing increases in productivity.

161 The conventional assumption is that the ACC structure began to develop during the Cenozoic, with the opening of the
162 Southern Ocean pathways between South America and Antarctica and the following formation of the Drake Passage
163 (DP) and, also between Australia and Antarctica that allows the Tasmanian Gateway (TG) opening. Removing these
164 geographic barriers permitted a gradual development of circumpolar flow (Toggweiler and Bjornsoon, 2000). The TG
165 opening to intermediate and deep waters occurred in the late Eocene, ca 35.5 Ma (Stickley et al., 2004). In contrast,
166 tectonic reconstructions for the timing of the Drake Passage opening remain controversial, ranging from the late Eocene
167 (ca 41 Ma; Scher and Martin, 2004, 2006) to the late Oligocene (ca 26 Ma, Barker and Thomas 2004, Hill et al., 2013)
168 for shallow water exchange. Some studies pointed to deep water exchange occurring as late as the earliest Miocene (ca
169 22-23 Ma, Barker 2001; Lyle et al., 2007). Even if the timing of the deepening of the Drake Passage is less well
170 constrained, a “proto-ACC” has been proposed as an earlier expression of the ACC and it is defined as a shallow-depth
171 circumpolar current (Scher et al., 2015, Sarkar, et al., 2019). Cramer et al. 2009 suggested that “proto-ACC” would
172 have played an important role in the ocean circulation changes that occurred in the Eocene. Furthermore, even a
173 relatively shallow proto-ACC would have strongly affected surface water phyto- and zooplankton (Lazarus and Caulet,
174 1994), and thus potentially the mechanisms of surface water productivity in the region.

175 Many climate model studies have contributed insights into the ocean structure and circulation of the late Eocene (e.g.
176 Huber et al. 2004, Huber & Not 2006, Sijp et al., 2011, Sijp et al., 2016, Elsworth et al., 2017, Baatsen et al., 2020;
177 Toumoulin, et al., 2020; Sauermilch et al., 2021; Nooteboom et al., 2022). Although some of these experiments have
178 shown that opening of gateways was not sufficient to have caused the global cooling recorded by proxies (DeConto &
179 Pollard, 2003, Huber et al. 2004, Huber & Not 2006, Sijp et al., 2011, Baatsen et al., 2020), they acknowledge that the
180 circulation patterns have changed during the Eocene. A recent model circulation experiment has demonstrated a
181 significant regional impact of the DP opening and its effects on ocean structure and dynamics even for shallow depths
182 (Toumoulin et al., 2020).

183 The organisation of Southern Ocean proto-oceanic fronts may have occurred during the late-Eocene as shown by
184 microfossil biogeographic data (Lazarus and Caulet, 1994; Cooke et al., 2002). This frontal system organization likely
185 played a role in major changes at that time period, including higher ocean productivity.

186 Evidence of significant events during the late Eocene highlights the importance of this period that preceded the
187 permanent glaciation in Antarctica. An interval of increasingly heavy global benthic oxygen isotope values in the late
188 Eocene, at ca 37 Ma have been interpreted to reflect pre-EOT glaciation and cooling, this episode is referenced as
189 PrOM event (Priabonian Oxygen isotope Maximum, Scher et al., 2014). Additional evidence for a prominent cooling
190 episode has been found during this time period (Anderson et al., 2011; Douglas et al., 2014). Despite uncertainties about
191 the nature and extent of the earliest ice in Antarctica, these changes imply that paleogeographic reconfiguration has
192 affected the late Eocene Antarctic climate and it is likely that a combination of processes favoured the development of
193 permanent glaciation in Antarctica.

194 Given the importance of changes during the Eocene-Oligocene time interval, especially the ACC development and its
195 frontal structure to the climate system and ecosystems, it is crucial to investigate the timing and magnitude of late
196 Eocene paleoceanographic changes in the Southern Ocean, and equally important to expand our understanding of the
197 implications of such changes on paleoproductivity and how these mechanisms are linked to a changing climate.

198 Our multiproxy approach and wide coverage allow us to test the hypotheses:

199 H1: Changes in ocean circulation patterns that took place during the late Eocene and early Oligocene (eg. development
200 of a proto-ACC and strengthening of AMOC) contributed to the increase in biological productivity in the Southern
201 Ocean.

202 H2: The export productivity increase that preceded the EOT may have been temporally correlated to, and thus may have
203 contributed to the drawdown of $p\text{CO}_2$.

204 First, we investigate the export productivity changes across the late Eocene to early Oligocene in three different regions
205 in the Southern Ocean. Then we compare our results to the paleo-circulation changes that occurred at the same time
206 period, and lastly compare our productivity records to the temporal pattern of change in Eocene-Oligocene $p\text{CO}_2$. We
207 conclude by summarising the implications of the changes in ocean circulation and the possible climate driving
208 mechanisms that led to the cooling of Earth.

209 **2 Materials and Methods**

210 **2.1 Site Descriptions**

211 We investigated sediment samples from 3 Ocean Drilling Program (ODP) Sites in the Southern Ocean (Table 1). ODP
212 Site 1090 on the southern flank of the Agulhas Ridge in the Southern Atlantic Ocean ($42^{\circ}54.8'S$, $8^{\circ}53.9'E$, water depth
213 $3,702\text{m}$), ODP Site 689 on the southern flank of the Maud Rise in the Southern Atlantic Ocean ($64^{\circ}31'S$, $3^{\circ}6'E$, water
214 depth $2,253\text{m}$) and ODP Site 748 on the southern part of the Kerguelen Plateau in the Southern Indian Ocean
215 ($58^{\circ}26.45'S$, $78^{\circ}58.89'E$, water depth $1,290.9\text{m}$). All the sites lie on topographic highs. The Agulhas Ridge comprises
216 an elongate part of the Agulhas-Falkland Fracture Zone (AFFZ). The ridge rises $\sim 3000\text{m}$ above the surrounding floor
217 and constitutes a topographic barrier, having a strong influence on the exchange of water masses (Gruetzner &
218 Uenzelmann-Neben, 2015) between high and lower latitudes. The Maud Rise is a seamount, its elevation rises almost
219 3000 m from the seafloor (Brandt et al., 2011). Kerguelen Plateau is a large topographic high in the Indian sector of the
220 Southern Ocean. We selected samples from the middle Eocene through the E-O boundary, depending on the sample
221 availability.

222 Currently, the sites studied are located in the Southern Ocean through the ACC. Site 689 is located well south of the
223 Polar Front Zone (PFZ), and 748 slightly to the south of the PFZ and Site 1090 in the Subantarctic zone, between the
224 Subtropical front (STF) and the Subantarctic Front (SAF) (Figure 1). Across the Eocene-Oligocene transition, the sites
225 were shallower (Table 1), ranging between ca 1.2 and 3 km paleo water depth. These depths are well suited to capture
226 signals of export productivity to intermediate-deep waters. Sites 689 and 748 locations were similar to today and site
227 1090 was as much as 5° farther to the south (Gersonde et al., 1999) (Table 1).

228 The major lithology from the lower Eocene to the upper Oligocene at the Maud Rise is composed of calcareous and
229 silicious oozes (Barker et al., 1988). Kerguelen Plateau site is composed mainly of nannofossil ooze and chert (Barron
230 et al., 1989). Agulhas Ridge is predominantly composed of diatoms and nannofossil ooze, with CaCO_3 wt% highly
231 variable, ranging from non-detectable to 69% of sediment throughout the study interval. (Gersonde et al., 1999) with

232 rare occurrences and barren intervals of planktic and benthic foraminifera making it difficult to establish stable isotope
 233 records at this site.

234 **Table 1.** Position of the ODP Sites studied in the present-day and in the late-Eocene (~ 37 Ma). Paleocoordinates
 235 calculated based on Seton et al. (2012) rotation model.

Site	Geographic Setting	Latitude	Longitude	Water depth (m)	Paleodepths (m)	Paleo-latitude	Paleo-longitude
1090	Agulhas Ridge	42°54.8'S	8°53.9'E	3 702	ca. 3,000-3,300 (Pusz et al. 2011)	ca 47°33'S	ca 1°46.8' E
689	Maud Rise	64°31'S	3°6'E	2 253	ca. 1500 (Diester-Haass and Zahn, 1996)	ca 64°19.2'S	ca 2°43.2' E
748	Kerguelen Plateau	58°26.45'S	78°58.89'E	1 290.9	ca. 1200 (Wright et al., 2018)	ca 56°48.6'S	ca 75°36' E

236 2.2 Age Models, Linear Sedimentation Rates

237 Revised age models for the ODP Site 1090, ODP Site 689 and ODP Site 748 made for this study were based on all
 238 magnetostratigraphic and biostratigraphic data available, and both models and data are available from the Neptune
 239 database-NSB system (Renaudie et al., 2020) (Figures S1-S4). All ages in our study are given in the GPTS standard
 240 used by NSB (Gradstein et al. 2012), or have been remapped to this scale from prior studies. Differences between this
 241 and more recent GPTS scales in the Cenozoic are minor, and generally less than other age model uncertainties for the
 242 sections in our study.

243 ODP Site 1090 has an age model constructed from shipboard magnetostratigraphic “U-channel” measurements, and the
 244 records fit well to the geomagnetic polarity timescale (GPTS) (Channell et al., 2003). Nannofossil biostratigraphy has
 245 confirmed the Chron ages (Marino and Flores, 2002), as well as foraminiferal biostratigraphy (Galeotti et al. 2002),
 246 strontium isotopes (Channell et al., 2003) and oxygen and carbon isotope data from benthic foraminifera (Zachos et al.,
 247 2001; Billups et al., 2002). This integration of several age indicators and their consistency makes this a robust and very
 248 well constrained age model.

249 Magnetostratigraphic data for ODP Site 689 is partially reinterpreted from the measurements originally made by Spiess,
 250 1990. A new high-resolution study of Eocene-Oligocene "U-channel" samples from this site shows a high correlation
 251 with the GPTS (Florindo and Roberts, 2005). Calcareous nannofossil datums (Wei and Wise, 1992; Wei, 1992, Persico
 252 and Villa, 2002, 2004), planktonic foraminiferal datums (Kennett and Sott, 1990; Thomas, 1990; Berggren et al., 1995)
 253 and Argon-argon ($^{40}\text{Ar}/^{39}\text{Ar}$) dating (Glass et al., 1986; Vonhof et al., 2000) are used to re-calibrate ages for this site.

254 A high-resolution magnetostratigraphic study from ODP Site 748B was carried out by Roberts et al. 2003 in continuous
 255 “U-channel” samples, revising the shipboard analysis from Inokuchi and Heider, 1992. Calcareous nannofossil
 256 biostratigraphy (Aubry 1992), planktonic foraminiferal biostratigraphic datums (Berggren et al., 1995), diatom datums
 257 (Baldauf and Barron, 1991, Roberts et al., 2003) and strontium isotope ages (Zachos et al., 1999; Roberts et al., 2003)
 258 were re-evaluated for a better age model.

259 Accumulation rate fluxes are obtained by calculating the product of linear sedimentation rates (LSR) and shipboard
260 measured dry bulk densities (DBD), thus a robust age model is crucial for this calculation because it determines the
261 linear sedimentation rates. We use a straightforward LSR calculation between age-depth control points based on
262 magnetostratigraphic data, stable isotopes and biostratigraphic data. Mass accumulation rates (MARs, $\text{mol cm}^{-2} \text{ kyr}^{-1}$)
263 were calculated using LSR based on the above age models multiplied by DBD.

264 Since bio-Ba AR is a direct function of LSR, it is essential to evaluate any possible biases due to this. Figure S5 shows a
265 comparison of linear sedimentation rates and bio-Ba AR. This comparison showed a high amplitude peak at ODP Site
266 1090, with LSR of 4.11 cm kyr^{-1} at the late Eocene, this high rate is based on a very constrained model. The LSRs for
267 ODP Site 689 vary from 0.1 cm kyr^{-1} during the early Oligocene to up to 1.3 cm kyr^{-1} in the late Eocene, whereas ODP
268 Site 748 has more uniform values during the late Eocene. The available age data for our sites allow some variation in
269 the placement of the line of correlation, and thus the precise timing and magnitude of sedimentation rate changes on the
270 scale of $\pm \text{ca } 0.5 \text{ m.y.}$ are not well constrained. Patterns and calculated values over longer time scales are however
271 thought to be robust.

272 **2.3 Stable Isotope Analyses**

273 Stable isotopes of carbon and oxygen were measured both on the bulk fine fraction ($<45\mu\text{m}$) and benthic foraminifera.
274 Bulk sediments were oven-dried and washed through different sieve sizes (125 and $45\mu\text{m}$). Smear slide observations
275 indicate that the main carbonate composition of the fine fraction is coccoliths, therefore stable isotopic compositions of
276 bulk fine fraction ($<45 \mu\text{m}$) reflect primarily nannofossil isotope signals. Contamination by non-coccolith carbonate
277 such as fragments of foraminifera shells is minimal (Figure S5). Fifteen to twenty tests of benthic foraminifera
278 (*Cibicidoides* spp.) were picked from the $>125\text{-}\mu\text{m}$ -size fraction. Foraminiferal tests were ultrasonically cleaned using
279 ethanol and oven-dried. Stable isotopic analyses were carried out at the Stable Isotope Laboratory of the Museum für
280 Naturkunde (Berlin, Germany) on a Thermo Isotope Ratio Mass Spectrometer. All values are reported in the δ -notation
281 in parts per mil (‰) relative to the Vienna Pee Dee Belemnite (VPDB). In this study, we applied an adjustment of
282 $+0.64\text{‰}$ (Shackleton and Opdyke, 1973; Shackleton et al., 1984) to all $\delta^{18}\text{O}$ values of the benthic foraminifera
283 *Cibicidoides* to account for disequilibrium effects.

284 **2.4 Barium Analyses and Biogenic Barium as a Paleoproductivity Proxy**

285 Barium (Ba) and aluminium (Al) were analysed by ICP OES, performed at the EIMiE Lab at the German Centre for
286 Geosciences (GFZ, Potsdam, Germany) using a 5110 spectrometer (Agilent, USA). The analytical precision and
287 repeatability were generally better than 2% and it is regularly tested by certified reference material and in-house
288 standards. For preparation, 2g of each sample was grounded to assure grain size distribution, and digested by Na_2O_2
289 fusion and HCl using ultrapure reagents, following the method by Bokhari and Meisel (2017). Intensity calibration was
290 performed by external calibration using the same batch of solvent to ensure matrix matching. The analytical blank was
291 negligible compared to the sample concentration.

292 Using barium as a paleoproductivity proxy requires some adjustments because other biogenic sources may contribute to
293 the barium content in the sediment. Detrital aluminosilicate may affect the barium signal in Southern Ocean sediments.
294 In order to solve this issue and reveal aluminosilicate contributions, the Biogenic Barium calculation was used as
295 proposed by Dymond et al., 1992, following Eq (1):

296 Biogenic Barium (Bio Ba) = (Ba total)_{sample} - (Ba/Al)_{bulk continental crust} × Al_{sample} (1)

297 This assumes that the aluminium (Al) concentration and the average continental crust abundance are representative of
298 the detrital Ba component. The Ba/Al crust ratio of 0.0075 is the global average value from sedimentary rocks as
299 suggested by Dymond et al. (1992). This value is based on various compilations of elemental abundances in crustal
300 rocks. This normative calculation potentially introduces uncertainty in samples with high and variable detrital barium,
301 but considering that clay assemblages and weathering regimes were relatively constant during the early Paleogene in the
302 Southern Ocean, therefore, the crustal ratio probably did not vary much (Robert et al. 2002).

303 2.5 Data Compilation

304 2.5.1 Neodymium Isotope Data

305 Neodymium isotopes in seawater reflect the different weathering sources of neodymium that affect each water mass.
306 The isotope values act as conservative elements during ocean mixing. They are therefore a robust water mass tracer, and
307 are faithfully archived in sediments (Piepgras and Wasserburg, 1982; Martin and Haley, 2000). Their behaviour in
308 seawater and the conservation of the signal in sediments make them a valuable proxy for paleoceanographic studies and
309 past ocean circulation reconstruction. Fossilised fish teeth are commonly used and considered robust archives to extract
310 Nd isotopic signatures because they incorporate and preserve their Nd signature during very early diagenesis (Martin
311 and Scher, 2004), and they can be found in deep-sea sediment samples all over the world and in many geologic time
312 intervals. The Nd signal is given in ϵNd , where ϵNd is the ratio $^{143}\text{Nd}/^{144}\text{Nd}$ of a sample relative to the same of the bulk
313 Earth, in parts per 10,000.

314 In this study, we compiled published Nd isotope data from fossil fish teeth, from the same Ocean Drilling Program
315 (ODP) sites that we investigated in the Southern Ocean (ODP Site 1090 Agulhas Ridge, Scher and Martin, 2006; ODP
316 Site 689 Maud Rise, Scher and Martin, 2004; and ODP Sites 738, 744 and 748 on the Kerguelen Plateau, Scher and
317 Delaney, 2010; Scher et al., 2011; Scher et al., 2014; Wright et al., 2018) and explore the Nd isotope variability to
318 examine the intrusion of waters from the Pacific to the Atlantic sector of the Southern Ocean. We then used these data
319 and our records to explore the evolution of the Southern Ocean circulation and significant circulation changes across the
320 Eocene-Oligocene transition. Sources of Nd isotope data are given in Table S1.

321 2.5.2 $p\text{CO}_2$ Data

322 A variety of geological proxies have been applied in numerous studies to reconstruct the partial pressure of atmospheric
323 CO_2 ($p\text{CO}_2$) during the Cenozoic Era (e.g. Pagani et al., 2005, 2011; Künschner et al., 2008; Retallack et al., 2009;
324 Beerling & Royer 2011, Anagnostou et al., 2016, 2020). Given the low published sampling density through the critical
325 Eocene-Oligocene interval, we compiled published $p\text{CO}_2$ data from marine and terrestrial proxies that have been
326 identified as reliable for reconstructing $p\text{CO}_2$ during this period. The marine geochemical proxies include alkenone-
327 based estimations, carbon and boron isotope ($\delta^{11}\text{B}$) composition of well-preserved planktonic foraminifera calcite.
328 Proxies from the terrestrial reservoir include Paleosols and Stomatal frequencies. Our atmospheric CO_2 compilation
329 (Table S2) consists to our knowledge all the currently available proxy data on Eocene and Oligocene $p\text{CO}_2$ records,
330 including all data compiled in previous syntheses through extensive scientific community efforts in paleo CO_2 database
331 (The Cenozoic CO_2 Proxy Integration Project Consortium, 2023), such compilations are commonly used to estimate

332 past $p\text{CO}_2$, although it is known that there are limitations and variation among them (IPCC, 2021). Zhang et al. (2013)
333 specifically argued that compositing limited, short time interval data from different proxies, and different localities is
334 likely to introduce significant short-term bias at individual data series end-points into the resulting fitted curve, and
335 instead generated a 40 My long history of Cenozoic $p\text{CO}_2$ using a single proxy from a single section (Site 925 in the
336 equatorial Atlantic). We consider this study's results to be the best and most complete single source of information on
337 the Cenozoic trend of atmospheric $p\text{CO}_2$. However, precisely because of the substantial amounts of between proxies and
338 between locality variation, data using a single proxy and from a single site is also potentially not representative of
339 global $p\text{CO}_2$ history. We thus use both the single site results of Zhang et al. (2013) and the full, multi-site and multi-
340 proxy compilation (Supplementary material) in evaluating our own study's results.

341 **3 Results**

342 **3.1 Biogenic Barium**

343 Biogenic Barium accumulation rate (bio-Ba AR) records (Figure 2) show a pronounced rise in the late Eocene when the
344 values were up to twice as high as in previous periods for all sites studied. At Kerguelen Plateau ODP Site 748, we also
345 observe a previous and smaller increase around the middle Eocene Climatic Optimum (MECO, ca 40 Ma). At Maud
346 Rise the increase began at ca 38.3 Ma and persisted for around 1.5 Myr. bio-Ba ARs show a high value in the Agulhas
347 Ridge at ca 36.8 Ma which is induced by a high sedimentation rate (Figure S5a). Although export productivity was
348 higher (maximum values to about $16.8 \mu\text{mol bio-Ba cm}^{-2} \text{ky}^{-1}$) at Maud Rise compared to the other sites -the Kerguelen
349 Plateau reached maximum values of about $14.3 \mu\text{mol cm}^{-2} \text{ky}^{-1}$ and the Agulhas Ridge site $13.74 \mu\text{mol cm}^{-2} \text{ky}^{-1}$, the
350 records show a high degree of temporal correspondence in the late Eocene peak (ca 36.8 Ma). Bio-Ba values were low
351 at all sites between ca 36 and 34.5 Ma. Between ca 34.5 Ma and ca 33.3 Ma, which includes the EOT interval, bio-Ba
352 AR increased in both sites of the Atlantic Sector, but these increases were not very concurrent between the sites
353 investigated. On the Agulhas Ridge, ODP Site 1090, the rise in bio-Ba (from 7.37 to $20.46 \mu\text{mol cm}^{-2} \text{ky}^{-1}$) is observed
354 in the very latest Eocene (ca 34.3), just before the Oi-1 event. At Maud Rise, ODP Site 689, the increase is not observed
355 until ca 1 Myr after, in the early Oligocene (maximum value $16.25 \mu\text{mol cm}^{-2} \text{ky}^{-1}$ at ca 33.3 Ma). On the Kerguelen
356 Plateau, ODP Site 748, the increase in export productivity registered by bio-Ba during the Oligocene is notably smaller
357 than in the Atlantic sites, with values not higher than the low values observed during the Eocene.

358 Our bio-Ba results are in general concordant with the temporally more limited data obtained by prior studies of
359 Southern Ocean sites (Anderson and Delaney, 2005, Site 1090; Diester-Haass and Faul 2019, Site 689) (Figure 2).
360 However, our results for Kerguelen Plateau Site 748 differ from those of Faul and Delaney, 2010 for nearby Site 738,
361 where the latter estimate bio-Ba accumulation rates up to twice those obtained in our study of Site 748. The differences
362 may be due to the different locations of the two sites, Site 738 is located several degrees further south, and in ca 1 km
363 deeper water depth. The bio-Ba proxy is also very sensitive to sedimentation rates, and the differences may be due to
364 the poor age control for Site 738 which in the studied time interval consists only of a few rather scattered
365 biostratigraphic events (Figure S4a), resulting in substantially different age models between our study, Faul and
366 Delaney (2010), and other recent studies of this site, e.g. Huber and Quillevere (2005). In these studies the location and
367 extent of hiatuses, and the uniformity of sedimentation rates varies considerably (SOM Figure S4b). The age model for
368 Site 748 by contrast (Figure S3) is very well constrained by coherent biostratigraphic events from multiple groups of

369 microfossils, Sr isotope stratigraphy and paleomagnetic stratigraphy, and we therefore accept the results from Site 748
370 as being more reliable.

371 When the data for individual sites is composited together, the behaviour of the Southern Ocean region can be roughly
372 estimated, even though our geographic coverage (lacking data from the Pacific/New Zealand sector) is incomplete and
373 thus may not be entirely representative of the Southern Ocean as a whole. A lowess curve fit to the composited bio-Ba
374 data shows that the key patterns noted in individual records are retained in the composite signal, and thus that Southern
375 Ocean productivity can be characterised as having had two intervals of high values at around 37 and 34 Ma.

376 **3.2 Oxygen and Carbon Isotopes**

377 Our new oxygen (Figure 3C and E) and carbon (Figure 3D and F) stable isotope data allow us to identify previously
378 noted trends and distinct events during the period studied. Benthic $\delta^{18}\text{O}$ values exhibit a consistent increasing trend
379 during the late Eocene indicating the overall decrease of oceanic bottom water temperatures. A sharp increase occurs at
380 the Eocene-Oligocene transition (between 33.9 and 33.3 Ma) at both sites examined. This rapid shift has been observed
381 in several sites in the Southern Ocean (e.g., Muza et al., 1983; Miller et al., 1987; Mackensen and Ehrmann, 1992;
382 Zachos et al., 1996; Billups et al., 2002; Pusz et al., 2011) and it is well established as a global signal (Zachos et al.,
383 2001). It is generally interpreted as a combination of deep ocean water cooling and major ice growth on the Antarctic
384 continent (Zachos et al., 2001). At Site 689, the planktic $\delta^{18}\text{O}$ curve almost mimics the benthic one. The $\delta^{18}\text{O}$ values
385 measured on fine fraction reveal a heavier trend more pronounced at ODP Site 748 (Kerguelen Plateau) compared to
386 ODP Site 689 (Maud Rise). During the late Eocene, around 37 Ma, heavier $\delta^{18}\text{O}$ values are observed in both the Atlantic
387 and Indian Sectors of the SO, the benthic/fine fraction ratio declines, indicating more homogenous temperature in the
388 water column. Both benthic and planktic foraminifera $\delta^{13}\text{C}$ records show fluctuations across the period studied, with
389 low values across the Eocene-Oligocene boundary, followed by an increase that accompanied the $\delta^{18}\text{O}$ increase and low
390 values again in the upper Oligocene. The benthic trend is also observed by previous data from the same sites
391 (Mackensen and Ehrmann, 1992; Diester-Haass and Zahn, 1996; Bohaty et al., 2003). The fine fraction records show
392 elevated $\delta^{13}\text{C}$ values between Late Eocene to Early Oligocene, followed by a decreasing trend during the Oligocene
393 (from ca 33.2Ma). At Site 748, the fine fraction $\delta^{13}\text{C}$ curve shows less fluctuation than the benthic curves during the
394 middle Late Eocene. A synchronous $\delta^{13}\text{C}$ increase (ca 0.6‰ shift) is observed at 36.5 Ma. Elevated fine fraction $\delta^{13}\text{C}$
395 values are observed from the late Eocene until the early Oligocene, coherent with previous studies (Bohaty et al., 2003),
396 while the benthic values stay low during the same period (Figure 3D and F).

397 **3.3 $p\text{CO}_2$ Proxies**

398 As noted above, given the complexities and potential biases of compiling data from different proxies and different time
399 intervals, we prefer to use the single site single proxy time series of $p\text{CO}_2$ from Zhang et al. (2013). This data (Figure 4)
400 shows two peaks in the late Eocene, with a maximum for the entire study interval at ca 37 Ma and a smaller peak at ca
401 34.5 Ma, and a rapid drop of over 200 ppm from nearly 1000 to ca 750 ppm in the earliest Oligocene (ca 33.5 Ma).
402 Despite the limitations of multi-proxy, multi-site compilations, the compiled data (Table S2; Figure S7) shows the same
403 basic features, nor does the result appear to be sensitive to the precise choice of data to include in the analysis.

404 **4 Discussion**

405 **4.1 Correlation of Productivity to Ocean Circulation, Glaciation and $p\text{CO}_2$ Change**

406 Intervals of high export productivity (bio-Ba) exhibit synchronous changes with intervals of changes in oxygen and
407 carbon stable isotopes and $p\text{CO}_2$ data (Figures 3 and 4). Notably, these intervals occur in the late-Eocene (~ 37 Ma) and
408 at the E/O boundary (~34 Ma). This correlation is highly suggestive that ocean circulation, glaciation, productivity and
409 atmospheric $p\text{CO}_2$ changes are interconnected. It could be assumed that (1) primary processes, such as ocean circulation
410 and glaciation are independently driving productivity and $p\text{CO}_2$ changes, or (2) a cascading effect, with glaciation and
411 ocean circulation influencing productivity and, consequently, altering atmospheric $p\text{CO}_2$ levels. While we cannot in our
412 study distinguish between these two possibilities, we explore the second, as proposed by Egan et al. (2013), in which
413 changes in ocean conditions due to tectonic-climate drivers affect productivity, and the latter in turn $p\text{CO}_2$ levels.

414 **4.2 Late Eocene Productivity Event and its Potential Impact**

415 The noticeable bio-Ba AR peak at ~ 36.8 Ma (Figure 2), suggests an important, ca 1 My long event of approximate
416 doubling of export productivity during the late Eocene, preceding the significant cooling and the first formation of large
417 Antarctic ice sheets at the Eocene-Oligocene boundary. The temporal synchronicity among different site locations in the
418 Southern Ocean suggests that the process driving this enhanced export productivity in the late Eocene occurred
419 throughout the Southern Ocean, requiring a mechanism that increased the delivery of nutrients to the surface ocean.

420 Our findings corroborate previous paleoproductivity studies that indicate an increase in export productivity in the
421 Atlantic Sector of the Southern Ocean during this time period. Anderson and Delaney (2005) found several peaks in
422 productivity indicators at the Agulhas Ridge during the same time interval, and benthic foraminiferal accumulation rates
423 show an increase in paleo-primary productivity on Maud Rise (Diester-Haass & Faul, 2019) (Figure 2). A pronounced
424 opal abundance peak is also documented by Diekman et al. (2004) between 37.5 and 33.5 Ma at the ODP Site 1090.
425 Our results now show that the 37 Ma event extended at least as far as the Kerguelen Plateau in the Indian Ocean sector,
426 with a substantial peak around 37 Ma and an earlier one near 40 Ma, thus affecting a large portion of the Southern
427 Ocean region.

428 A direct analysis of the impact of the potential significance of this event for the development of late Eocene global
429 climate depends on two key factors: the extent to which the increased productivity contributed to enhanced carbon
430 sequestration, and the magnitude of sequestration over the ca 1 my interval of enhancement. Understanding the impact
431 of productivity on carbon sequestration for the Eocene oceans however is complicated by the lack of knowledge of
432 several factors that influence this process. These factors include our ability to estimate the impact of higher productivity
433 on carbon sequestration is limited, as many of the factors that affect this in the modern ocean are poorly understood for
434 Eocene oceans (export efficiency to the subsurface waters, rates of transport and degradation in the water column and
435 upper sediment layers, organic carbon content of Southern Ocean Eocene pelagic sediments; as well as transport of
436 organic carbon by subsurface water layers in the late Eocene oceans to lower latitude areas of productivity and
437 sequestration. We therefore cannot directly calculate the impact that the observed productivity change had on $p\text{CO}_2$.
438 Instead we take an indirect approach, comparing the productivity history to the history of $p\text{CO}_2$ and potential drivers of
439 productivity change such as ocean circulation and climate change.

440 **4.3 Surface Water Changes in Physical Conditions in the Late Eocene**

441 The late Eocene is generally accepted as a time interval of gradual cooling of Southern Ocean waters. Indeed,
442 biomarker-based temperature estimates reveal substantial (3-5 °C) high latitude sea surface temperatures (SST) cooling
443 within the late Eocene (Liu et al., 2009; O'Brien et al., 2020). Our fine fraction stable oxygen isotopes confirm this
444 cooling trend following MECO, with a distinct peak at 37 Ma during the Eocene, matching the peak cooling reported by
445 O'Brien et al. (2020). This interval of maximum $\delta^{18}\text{O}$ values occurred during the same interval in which export
446 productivity increased (Figure 2). In this interval the difference in the $\delta^{18}\text{O}$ gradient between benthic foraminifera and
447 fine fraction (nannofossil) carbonate is less pronounced. This increase in similarity is interpreted as having been caused
448 by a decrease in water column stratification and enhanced vertical mixing.

449 This change in export productivity in the late Eocene is coeval with a change towards increasing variability of carbon
450 stable isotopes ($\delta^{13}\text{C}$) of benthic foraminifera (Figure 4). Although $\delta^{13}\text{C}$ in individual sections can also represent local
451 effects, usually there is a strong component of global changes in carbon reservoirs, and indeed our local measurements
452 closely align with the global curve (Figure 3B, D and F). In the global context, a shift towards more positive values in
453 the benthic $\delta^{13}\text{C}$ at ~ 37 Ma indicates a carbon cycle perturbation. This shift coincides with the export productivity
454 changes observed in our study. One possible explanation is that higher productivity may have elevated the export flux of
455 organic carbon to sediments, thereby increasing the marine organic carbon burial and preferentially scavenging the
456 lighter ^{12}C from the carbon pool.

457 **4.4 Oceanographic Circulation Drivers of the Late Eocene Productivity Change**

458 We propose that the main cause for the productivity increase observed in the late Eocene is the upwelling of nutrient-
459 rich deep waters. Understanding however the physical oceanographic mechanisms that led to increased upwelling
460 throughout the Southern Ocean requires examining links between the different processes that occurred at that time
461 period. Changes in paleoceanography during the Paleogene were significantly mediated through tectonic re-
462 organisation, such as the Southern Ocean gateways opening (i.e., the Drake Passage and the Tasman Gateway), changes
463 in the Atlantic-Arctic gateway and in the Tethys Seaway.

464 In this context, the Southern Ocean circulation during this time period is still debated due to uncertainties concerning
465 the opening of the gateways that led to the development of the Antarctic Circumpolar Current (ACC). Estimates for the
466 onset of the modern-like ACC have not reached a consensus yet and vary from as early as middle Eocene (ca 41 Ma,
467 Scher & Martin, 2006; ca 35.5 Ma, Stickley et al. 2004) to middle Oligocene (ca 23Ma; Pfuhl and McCave, 2005). This
468 inconsistency suggests that the onset of ACC could have been a gradual or an intermittent change. Further, local proxy
469 records cannot distinguish between regionally developed fronts and true circumpolar flow (i.e. ACC).

470 In addition to $\delta^{18}\text{O}$ and $\delta^{13}\text{C}$, ϵNd has been used to identify circulation changes and water masses exchange through the
471 Eocene (Scher and Martin, 2004, 2008; Scher et al., 2014; Huck et al., 2017; Wright et al., 2018). Nd isotopes are one of
472 the most robust tracers of water mass origin (Frank, 2002). The residence time of Nd in oceans is much shorter (300-
473 1000 years) than ocean mixing time and is thus distinct at a given location. Further, the isotope composition of the Nd
474 ocean budget is solely determined by terrigenous contribution. The latter is balanced by Nd sinks that remove Nd
475 quantitatively, yet this only influences the net budget and thus the magnitude and/or swiftness of changes to the ϵNd
476 composition. However, mixing of water masses, e.g. through lateral or vertical mixing, can also cause changes as long
477 as they occur more rapidly than the residence times.

478 In the late Eocene, starting at 37 Ma, Scher and Martin (2004) found a dramatic positive shift in ϵ -Nd values in the
479 Atlantic sector of the SO that they interpreted as the influx of Pacific deep waters, due to its characteristic of more
480 radiogenic (positive) waters, not previously observed in the Atlantic Ocean. Recently published Nd isotope records from
481 the Kerguelen Plateau (Wright et al., 2018) revealed a long-term negative trend during the late Eocene, which also
482 suggests that the water mass mixing between the Pacific and Atlantic preceded 36 Ma. ϵ Nd (t) records from the
483 Kerguelen Plateau in fact showed values comparable to modern CDW during the Oligocene, inferring water mass
484 composition similar to the present day. Thus, Nd isotope data support at least partial opening of Drake Passage by the
485 late Eocene (before 36 Ma), consistent with plate tectonic reconstructions (Livermore et al., 2005, 2007). Regardless of
486 the depth, Neodymium isotope evidence for late Eocene opening of the Drake Passage suggests that increased fetch for
487 surface flow and changing deep water composition could have had changes in the surface water conditions in the South
488 Atlantic sector of the late Eocene Southern Ocean.

489 This has been explicitly demonstrated in a recent modelling study conducted by Toumoulin et al. (2020). They
490 demonstrate that the Drake Passage opening, even at shallow depth, notably connects prior regional frontal systems
491 together, thereby allowing the formation of a proto-ACC; and has a strong effect on the Southern Ocean Eocene water
492 mass structure, inducing ocean cooling in most of the Southern Hemisphere. These temperature changes are not linear
493 and differ from one region to another, with DP opening causing changes in the mixed layer depths and provoking
494 different responses in the Atlantic and Indian Sectors of the SO. In the Atlantic and Indian Ocean sectors in particular,
495 very deep seasonal mixing (several hundred meters) over broad areas of the entire region is replaced by more moderate
496 levels of mixing (generally ca 200 m or less), except near the proto-polar front region, where seasonal mixing of 300-
497 400 m still occurs. Vila et al. 2014 have found nannofossil assemblages characteristic of cool sea surface waters in the
498 late-Eocene in Kerguelen Plateau samples. Cooler temperatures are coeval with the paleoceanographic re-organization
499 and intensified upwelling that we infer for this time period, while differences in the depth of the mixed layers between
500 ocean basins may explain the different magnitude of export productivity observed in the Atlantic and Indian sectors of
501 the SO.

502 The wind-driven eastward flow and the characteristic fronts of the modern ACC support the upwelling of nutrient-rich
503 water to the surface and consequently high levels of productivity. On the balance of evidence, it seems that the export
504 productivity seen in our data in the late Eocene is likely to have occurred in response to a proto-ACC front's
505 development and its associated upwelling. The inferred onset of a proto-ACC in the late Eocene and our finding of
506 increased upwelling fits the hypothesis that ACC type circulation itself helps drive the AMOC circulation (Toggweiler
507 and Bjornsson, 2000; Katz et al., 2011; Sarkar et al., 2019). A proto-ACC causes SO upwelling, and thus provides
508 support for increasing AMOC-like circulation in the late Eocene as an additional cause of increased upwelling as a
509 causative mechanism of the export productivity event. Temperature asymmetry between Northern and Southern
510 Hemisphere and comparisons between benthic $\delta^{13}\text{C}$ records provide evidence for the strengthening of the AMOC in the
511 late Eocene (Elsworth et al., 2017).

512 **4.5 Eocene-Oligocene Boundary Productivity Changes**

513 The earliest Oligocene, following the E/O boundary, has been suggested as a period of a significant rise in biological
514 productivity in high southern latitudes (Diester-Haass, 1995, 1996; Diester-Haass and Zahn, 1996, 2001). However, in
515 contrast to the late Eocene event, the export productivity changes across the Eocene-Oligocene boundary observed in

516 our study were not always concurrent between the sites investigated (Figure 2). In the Atlantic sites, export productivity
517 increases and decreases several times from the late Eocene to early Oligocene. We thus argue that the fluctuations in
518 export productivity that occurred in the Southern Ocean during this global climatic re-organization are more strongly
519 modulated by local parameters, whereas the late Eocene productivity event is more uniform and reflects the global re-
520 organization of ocean circulation. If the trends observed in export productivity across the EOT were regulated only by
521 global, or at least regional temperature and circulation changes, then we would observe significant changes also in the
522 Indian sector of the Southern Ocean. It seems however that productivity increase was more pronounced in the Atlantic
523 sector of the Southern Ocean.

524 Today, the Southern Ocean (SO) has a frontal system that strongly impacts circulation, primary productivity and the
525 entire climate system (Chapman et al., 2020). The Antarctic Polar Front (APF) is particularly important for controlling
526 nutrient distribution. Latitudinal variations of the APF for example have been shown to alter regional productivity over
527 the glacial cycles (Kim et al., 2014, Thole et al., 2019). The causes of the lack of significant export productivity changes
528 in the Indian sector of the Southern Ocean during the early Oligocene after the Eocene-Oligocene boundary are unclear.
529 The Kerguelen Plateau may not have been located in a position favourable to nutrient-rich upwelling. In addition, the
530 regional frontal migration may have been more intense in the Atlantic sector compared to the Indian sector of the SO.

531 **4.6 A Scenario for Southern Ocean Productivity and Circulation Change in the Late Eocene**

532 The patterns of productivity change seen in our study can be placed in an (admittedly speculative) scenario, which is at
533 least compatible with prior studies and modelling of conditions in the late Eocene austral ocean region and Antarctica.
534 In the earliest interval covered in our study (ca 40-38 Ma) productivity was in most sites fairly low (Figure 5a). At this
535 time there is little evidence for a significant influx of Pacific waters into the Atlantic, and the Drake Passage is thus
536 assumed to be effectively closed to ocean circulation.

537 During the 38-36 Ma interval, evidence summarised by Scher et al. (2014) suggests that a significant, if transient,
538 glaciation event occurred on the Antarctic continent-the Priabonian oxygen maximum, or PriOM. If sufficient in
539 magnitude this would have significantly affected circulation throughout the austral ocean region, with strengthened
540 temperature gradients, invigorated circulation (Houben et al., 2019), and increased upwelling (Goldner et al, 2014). This
541 would account both for the substantial increase in productivity, and the broad geographic extent of the increase seen in
542 our data (Figure 5b). The cause of this glaciation event is unknown, but may be related in part to the trend in the late
543 Eocene towards lower atmospheric $p\text{CO}_2$ interacting with orbital fluctuations in polar insolation as explored in model
544 simulations by Van Breedam et al. (2022).

545 With the end of transient glaciation, the atmospheric forcing of ocean circulation would have declined, and with it the
546 high levels of productivity seen in our data (Figure 5c). However, by this time (ca 36-34 Ma) the Nd isotope data
547 suggests that a significant influx of Pacific water was reaching the South Atlantic sector of the austral ocean (Scher and
548 Martin, 2004), and consequently, the Drake Passage must have been at least partially open. This would have resulted in,
549 if not as strong as during the PriOM, nonetheless stronger circumpolar circulation in a proto-ACC, increased upwelling,
550 and increased nutrient availability from Pacific-sourced deep waters. The locus of high productivity would have become
551 however more cantered near the proto-ACC, which at that time, according to the model results of Toumoulin et al.
552 (2020) was located a few degrees north of the current location of the ACC. The high productivity and accumulation of
553 biogenic opal seen at Site 1090, fortuitously located at this time in this region can be thus be explained, as can the lower

554 relative productivity of Site 689, located much further to the south and thus outside the region primarily influenced by
555 the proto-ACC system.
556 Lastly, at the E/O boundary itself (Figure 5d), the well known major shifts in oxygen isotopes signal the formation of a
557 full continental ice-sheet, which would have in turn driven a renewed increase in circumpolar ocean circulation- a full,
558 if early form of the ACC, and dramatically increased levels of productivity, again however primarily near the ACC
559 region.

560 **4.7 Possible Implications to the EOT Global Cooling**

561 Our $p\text{CO}_2$ compilation shows that carbon dioxide levels declined gradually from ca 1200 ppm in the late Eocene to ca
562 750 ppm across the EOT (Figure 4 and Figure S7). There are different processes involved in the oceanic uptake of CO_2 .
563 The solubility pump is a physical-chemical process that promotes gas transfer between the atmosphere and seawater in
564 order to achieve chemical equilibrium. This process depends on temperature, in which the solubility increases as
565 temperature decreases. Evidence for cooling of surface waters observed in the Southern Ocean (Liu et al., 2009;
566 Hutchinson et al., 2021) could have favoured the ability to dissolve atmospheric CO_2 , contributing to the drawdown of
567 $p\text{CO}_2$ during the late-Eocene.

568 Silicate weathering has been suggested to play an essential role in regulating CO_2 across the EOT (Zachos and Kump,
569 2005). On geologic time scales, chemical silicate weathering is considered to modulate atmospheric CO_2 levels through
570 a negative feedback mechanism (Berner et al., 1983). Weathering of silicate rocks provides alkalinity to the oceans,
571 acting as a sink for atmospheric CO_2 , thereby influencing global climate. In addition, increasing silicate weathering
572 enhances primary productivity through the delivery of nutrients to the ocean. Intensified weathering is supported by Os
573 isotope records, showing an anomaly before the EOT, at ca 35.5Ma (Dalai et al., 2006).

574 High export productivity potentially modulates CO_2 by two major mechanisms, operating over very different time
575 scales. Productivity maintains a gradient in dissolved CO_2 between the surface and deep ocean by exporting organic
576 carbon from the surface into deep ocean waters, This in turn lowers the concentration of CO_2 in surface waters, causing
577 more atmospheric CO_2 to be drawn out of the atmosphere into dissolved surface ocean CO_2 . It is estimated that this
578 mechanism causes $p\text{CO}_2$ to be approximately 200 ppm lower than it would in a purely abiotic ocean (Volk and Hoffert
579 1985). In the second mechanism, in areas of the ocean with high export productivity a (generally rather small) fraction
580 of biologically captured carbon (both soft tissue and carbonate from coccolithophores and planktic foraminifera)
581 escapes remineralization in the water column and is buried in ocean bottom sediments, where it is sequestered for
582 (typically) many millions of years. Changes in either mechanism can contribute to the decline of atmospheric carbon
583 dioxide, thereby intensifying the cooling trend. Therefore, the observed increase in export productivity in the late-
584 Eocene over 1 My in multiple sites in the SO, and the temporal correlation with the changes in $p\text{CO}_2$ proxy records
585 showed in our study is compatible with the hypothesis proposed by Egan et al., 2013. This suggests that the heightened
586 export productivity identified in our study is a potential candidate that may have provided important positive feedback
587 to the $p\text{CO}_2$ decline.

588 However, this correlation is suggestive rather than conclusive, given the complexities of the carbon cycle. For instance,
589 variations in the efficiency of the carbon pump, remineralization (Griffith et al., 2021), the relationship between
590 nutrients availability and plankton utilization and the dynamics of shelf-deep sea carbonate (Sluijs et al., 2013) can
591 significantly influence the relationship between export productivity and $p\text{CO}_2$ levels and adds complexity to our

592 understanding. Limited data for the late-Eocene on some critical parameters to our understanding (e.g. sedimentary C_{org} ,
593 Olivarez Lyle & Lyle, 2006) further contributes to the uncertainties in establishing a causal link. Moreover, it is
594 essential to note that upwelling, while promoting nutrient-rich conditions favourable to productivity and the long-term
595 sequestration mechanism, also contribute to outgassing of CO_2 into atmosphere, influencing the carbon balance in the
596 short-term mechanism. This adds another layer of complexity to the carbon cycle dynamics and its relationship with
597 productivity changes. While our findings propose a potential link, it is crucial to recognize that this alone does not
598 constitute proof of the export productivity directly influenced late Eocene pCO_2 levels.

599 Despite some modelling studies showing that circulation changes were not the main factor in driving the cooling and
600 glaciation on Antarctica (e.g. Huber et al., 2004; Huber and Not 2006; Sijp et al., 2011), circulation changes still had a
601 significant impact, with e.g. Southern Ocean sea surface temperature declines of 2-4°C (Toumoulin et al., 2020),
602 affecting the atmosphere-ocean CO_2 equilibrium. A succession of events may have contributed to the evolution of
603 climate: thermal isolation of Antarctica, glacier formation, increasing intensity of silicate weathering, together with
604 upwelling of nutrient rich and cold deep waters, leading to high biological productivity, then declining pCO_2 . Moreover,
605 because the Atlantic Meridional Overturning Circulation (AMOC) affects the distribution of tracers such as
606 temperature, dissolved inorganic carbon (DIC), alkalinity and nutrients (Boot et al., 2021), the strengthening of AMOC
607 could explain the further decrease in atmospheric CO_2 via biological export productivity. Elsworth et al., (2017), for
608 example, suggest that enhanced weathering is driven by intensified AMOC in the latest Eocene due to increasing
609 AMOC causing differential global distribution and increase of surface temperatures and precipitation over land areas.
610 These factors together suggest that E-O changes in AMOC also may play an important role as a driver of CO_2 decline.
611 Taken together, the above processes indicate that a variety of positive feedback contributed to Antarctic glaciation from
612 about 37 Ma onwards. Recent evidence suggests that continental-scale Antarctic glaciation initiated in the late Eocene
613 (Scher et al., 2014; Carter et al., 2017). Our results indicate that significant changes in Southern Ocean export
614 productivity preceded the E/O boundary by approximately 3 million years. These trends are likely to be a response to
615 the combination of the intensified processes that had been in place since the late Eocene. The correlation between our
616 Southern Ocean productivity peaks and decline in global pCO_2 records suggest that biological productivity may have
617 played an important role in the drawdown of pCO_2 levels. Specifically enhanced CO_2 fixation by phytoplankton and
618 carbon sequestration in seafloor sediments increased via an increase in the biological pump may have contributed to
619 decrease atmospheric CO_2 , and through a positive feedback from declining Southern Ocean surface water temperature
620 enhanced boosting the cooling trend. The establishment of Antarctic glaciation may thus have been influenced
621 significantly by enhanced productivity.

622 **4.8 Limitations and Future Directions**

623 Our study has numerous limitations. Our data on paleoproductivity does not cover the full time interval in all of the sites
624 studied, and our geographic coverage is still incomplete. In particular, we have not examined sections from the Pacific
625 sector, or the influence of the Tasman gateway. Most of our interpretations are based on a single productivity proxy -
626 biogenic Barium. While this proxy is well established and gives coherent results in our study, productivity proxies are
627 known to have complex behaviours, and results using different proxies might be at least somewhat different. Our
628 suggestion that elevated late Eocene Southern Ocean productivity might have affected global carbon sequestration is
629 only a speculation based on general characteristics of the ocean carbon system, and much more detailed study of both

630 actual sequestration values in sediment, and the impact on atmospheric $p\text{CO}_2$ are still needed. Our interpretative
631 scenario attributing productivity changes to a combination of Drake Passage opening and continental scale glaciation on
632 Antarctica are also purely qualitative and need further study. Despite these limitations, our study sheds new light on the
633 late Eocene oceanic precursors of the Eocene-Oligocene glaciation event-the most dramatic climate change of the
634 Cenozoic.

635 **5 Conclusions**

636 Our bio-Ba data provide important records of the Southern Ocean productivity history across the EOT. These data show
637 that export productivity increased significantly in the late Eocene in the Southern Ocean and was affected by ocean
638 circulation changes. The development of a regionally varying circumpolar polar flow (proto-ACC) and the associated
639 frontal system proposed by other recent studies is likely to have contributed to the enhanced productivity in the
640 Southern Ocean through the intensification of upwelling (H1).

641 Our results show that increasing Southern Ocean productivity in the late Eocene to earliest Oligocene is correlated to
642 global changes in atmospheric $p\text{CO}_2$ and carbon isotope proxies for organic carbon extraction. This finding points
643 toward a potential positive climate system feedback, involving ocean circulation changes, enhanced export productivity
644 and drawdown of atmospheric CO_2 . Although many studies of the Eocene-Oligocene climate transition try to identify a
645 single dominant mechanism (e.g. ocean gateway opening vs $p\text{CO}_2$ decline) for causing the initiation of Antarctica
646 glaciation, each mechanism plays a different role and has associated complex feedbacks. Our study points toward a
647 climate feedback system involving ocean circulation, thermal isolation and biological productivity, where several
648 mechanisms are interconnected and cannot be considered separately. Openings of gateways led to the development of a
649 circumpolar flow, promoting cooling and increased upwelling that contributed to enhanced ocean carbon pump activity
650 and the decline of atmospheric carbon dioxide.

651 **Data Availability**

652 The supplementary information related to this article is available in the Supplement, the raw data will be available upon
653 publication in an open-access database (PANGAEA: <https://www.pangaea.de>).

654 **Author Contributions**

655 The manuscript was designed and written by GRF in collaboration with DL. DL updated age models. GRF prepared all
656 the samples for geochemical analyses. JS ran the barium and aluminium analyses. US generated carbon and oxygen
657 stable isotope data. $p\text{CO}_2$ data and neodymium isotopes data were compiled by GRF. Biogenic barium was calculated
658 by GRF. All authors contributed to editing the manuscript.

659 **Competing Interests**

660 The authors declare that they have no conflict of interest.

661 **Acknowledgments**

662 This study was funded by the Federal Ministry of Education and Research (BMBF) under the “Make our Planet Great
663 Again, German Research Initiative”, grant number 57429681, implemented by the German Academic Exchange Service
664 (DAAD).

665 References

- 666 Anagnostou, E., John, E. H., Edgar, K. M., Foster, G. L., Ridgwell, A., Inglis, G. N., Pancost, R. D., Lunt, D. J., and
667 Pearson, P. N. Changing atmospheric CO₂ concentration was the primary driver of early Cenozoic climate, *Nature*,
668 v. 533, pp. 380-384. <https://doi.org/10.1038/nature17423>, 2016.
- 669 Anagnostou, E., John, E. H., Babila, T.L., Sexton, P. F., Ridgwell, A., Lunt, D.J., Pearson, P.N., Chalk, T.B., Pancost,
670 R.D. and Foster, G.L. Proxy evidence for state-dependence of climate sensitivity in the Eocene greenhouse. *Nature*
671 *Communications*, 11, 4436 (2020). <https://doi.org/10.1038/s41467-020-17887-x>, 2020.
- 672 Anderson, L.D. & Delaney, M.L. Middle Eocene to early Oligocene paleoceanography from Agulhas Ridge, Southern
673 Ocean (Ocean Drilling Program Leg 177, Site 1090). *Paleoceanography and Paleoclimatology*, 20, 1.
674 <https://doi.org/10.1029/2004PA001043>, 2005.
- 675 Anderson, J.B., Warny, S., R.A. Askin, J.S. Wellner, S.M. Bohaty, A.E. Kirshner, D.N. Livsey, A.R. Simms, T.R. Smith,
676 W. Ehrmann, L.A. Lawver, D. Barbeau, S.W. Wise, D.K. Kulhanek, F.M. Weaver, W. Majewski. Progressive
677 Cenozoic cooling and the demise of Antarctica's last refugium, *PNAS*, 108, pp. 11356-11360, 2011.
- 678 Archer, D., Winguth, A., Lea, D., Mahowald, N. What caused the glacial/interglacial atmospheric pCO₂ cycles? *Reviews*
679 *of Geophysics*, 38 (2), 159-189. <https://doi.org/10.1029/1999RG000066>, 2000.
- 680 Arrhenius, S. On the influence of carbonic acid in the air upon the temperature of the ground. *Philosophical Magazine*
681 *and Journal of Science*, 5, v.41, 237-276, 1986.
- 682 Aubry, M.P. Late Paleogene Calcareous nannoplankton evolution: a tale of climatic deterioration In: Prothero, D.R.,
683 Berggren, W.A. (Eds.), *Eocene/Oligocene Climatic and Biotic Evolution*, Princeton University Press, Princeton, NJ,
684 pp.272-309, 1992.
- 685 Baatsen, M., Heydt, A. S. V. D., Huber, M., Kliphuis, M. A., Bijl, P. K., Sluijs, A., & Dijkstra, H. A. The middle to late
686 Eocene greenhouse climate modelled using the CESM 1.0.5. *Climate of the Past*, 16, 2573–2597.
687 <https://doi.org/10.5194/cp-16-2573-2020>, 2020.
- 688 Baldauf, J. G., & Barron, J. A. 29. Diatom Biostratigraphy: Kerguelen Plateau and Prydz Bay regions of the Southern
689 Ocean. In: Barron, J., Larsen, B. et al. (1991) *Proceedings of the Ocean Drilling Program, Scientific Results*, v 119,
690 1991
- 691 Barker, P.E, Kennett, J.P., et al. Proc. ODP, Init. Repts., 113: College Station, TX (Ocean Drilling Program).
692 doi:10.2973/odp.proc.ir.113.1988.
- 693 Barker, P.F. Scotia Sea regional tectonic evolution: implications for mantle flow and palaeocirculation. *Earth-Science*
694 *Reviews*, 55, 1-39 [https://doi.org/10.1016/S0012-8252\(01\)00055-1](https://doi.org/10.1016/S0012-8252(01)00055-1), 2001
- 695 Barker, P. and Thomas, E. Origin, signature and palaeoclimatic influence of the Antarctic Circumpolar Current, *Earth-*
696 *Science Reviews*, 66, 143–162, 2004.
- 697 Barron, J., Larsen, B., et al. Proc. ODP, Init. Repts., 119: College Station, TX (Ocean Drilling Program).
698 doi:10.2973/odp.proc.ir.119. 1989.
- 699 Beerling, D., Royer, D. Convergent Cenozoic CO₂ history. *Nature Geoscience*, 4, 418–420
700 <https://doi.org/10.1038/ngeo1186>, 2011.
- 701 Berggren, W.A., Kent, D.V., Swisher, C.C., III, and Aubry, M.P. A revised Cenozoic geochronology and
702 chronostratigraphy, in Berggren, W.A., et al., eds., *Geochronology, time scales and global stratigraphic correlation:*
703 *Framework for an historical geology: SEPM (Society for Sedimentary Geology) Special Publication 54*, p. 129–212,
704 1995.
- 705 Berner, R. A., Lasaga, A. C. & Garrels, R. M. The carbonate-silicate geochemical cycle and its effect on atmospheric
706 carbon dioxide over the past 100 million years. *Am. J. Sci.* 283, 641–683, 1983.
- 707 Bijl, P.K., Houben, A. J. P., Schouten, S., Bohaty, S. M., Sluijs, A., Reichert, G.-J., Sinninghe Damste, J.S., and
708 Brinkhuis, H. Transient Middle Eocene atmospheric CO₂ and temperature variations, *Science*, 330, 819-821, 2010.
- 709 Billups, K., Channell, J.E.T. and Zachos, J. Late Oligocene to early Miocene geo- chronology and paleoceanography
710 from the subantarctic South Atlantic, *Paleoceanography*, 17(1), 1004. doi:10.1029/2000PA000568, 2002.
- 711 Bohaty, S. M. and Zachos, J. C. Significant Southern Ocean warming event in the late middle Eocene, *Geology*, 31,
712 1017–1020, <https://doi.org/10.1130/G19800.1>, 2003.
- 713 Bohaty, S. M., Zachos, J.C., and Delaney, M.L. Foraminiferal Mg/Ca evidence for Southern Ocean cooling across the
714 Eocene-Oligocene transition, *Earth Planetary Science Letters*, 317–318, 251–261, 2012.
- 715 Boot, D., Von Der Heydt, A.S., and Dijkstra, H.A. Effect of the Atlantic Meridional Overturning Circulation on
716 Atmospheric pCO₂ variations. *Earth System Dynamics*, <https://doi.org/10.5194/esd-13-1041-2022>, 2022

- 717 Brandt, A., Bathmann, U., Brix, S., Cisewski, B., Flores, H., Göcke, C., et al. Maud Rise – A snapshot through the water
718 column. *Deep Sea Res. II*, 58, 1962–1982. doi: 10.1016/j.dsr2.2011.01.008, 2011.
- 719 Breecker, D. & Retallack, G. Refining the pedogenic carbonate atmospheric CO₂ proxy and application to Miocene
720 CO₂. *Palaeogeography, Palaeoclimatology, Palaeoecology*, 406, 1-8. <https://doi.org/10.1016/j.palaeo.2014.04.012>,
721 2014.
- 722 Carter, L., McCave, I.N., Williams, M.J.M. Chapter 4 Circulation and Water Masses of the Southern Ocean: A Review,
723 Developments in Earth and Environmental Sciences, *Elsevier*, v. 8, 85-114, [https://doi.org/10.1016/S1571-9197\(08\)00004-9](https://doi.org/10.1016/S1571-9197(08)00004-9), 2008.
- 724 Carter, A., Riley, T.R., Hillenbrand, C.D., Rittner, M. Widespread Antarctic glaciation during the Late Eocene, *Earth
725 and Planetary Science Letters*, 458, 49-57, <https://doi.org/10.1016/j.epsl.2016.10.045>, 2017.
- 726 Channell, J. E. T., Galeotti, S., Martin, E.E., Billups, K., Scher, H.D., and Stoner, J.S. Eocene to Miocene
727 magnetostratigraphy, biostratigraphy and chemostratigraphy at ODP Site 1090 (sub-Antarctic South Atlantic), *Geol.
728 Soc. Am. Bull.*, 115, 607–623, 2003.
- 729 Chapman, C.C., Lea, MA., Meyer, A. Defining Southern Ocean fronts and their influence on biological and physical
730 processes in a changing climate. *Nature Climate Change*, 10, 209–219, <https://doi.org/10.1038/s41558-020-0705-4>,
731 2020.
- 732 Clark, W. C. (ed.). Carbon Dioxide Review: 1982, p. 468, *Oxford University Press*, New York, 1982.
- 733 Cooke, P.J., Nelson, C.S., Crundwell, M.P., Spiegler, D. Bolboforma as monitors of Cenozoic palaeoceanographic
734 changes in the Southern Ocean, *Palaeogeography, Palaeoclimatology, Palaeoecology*, Volume 188, Issues 1–2, 73-
735 100, [https://doi.org/10.1016/S0031-0182\(02\)00531-X](https://doi.org/10.1016/S0031-0182(02)00531-X), 2002.
- 736 Coxall, H.K., Wilson, P.A., Pälike, H., Lear, C.H., Backman, J. Rapid stepwise onset of Antarctic glaciation and deeper
737 calcite compensation in the Pacific Ocean. *Nature*, 433, 53–57. <https://doi.org/10.1038/nature03135>, 2005.
- 738 Coxall, H., Pearson, P.N. The Eocene-Oligocene transition, In: Williams, M., Haywood, A.M., Gregory, F.J., Schmidt,
739 D.N. (Eds.), *Deep-Time Perspectives on Climate Change: Marrying the Signal from Computer Models and
740 Biological Proxies*. pp. 351–387, 2007.
- 741 Coxall, H. K., & Wilson, P. A. Early Oligocene glaciation and productivity in the eastern equatorial Pacific: Insights
742 into global carbon cycling, *Paleoceanography*, 26, PA2221, <https://doi.org/10.1029/2010PA002021>, 2011.
- 743 Dalai, T.K. et al. The Late Eocene 1870s/1880s excursion: Chemostratigraphy, cosmic dust flux and the Early
744 Oligocene glaciation. *Earth and Planetary Science Letters*, 241(3-4), 477-492,
745 <https://doi.org/10.1016/j.epsl.2005.11.035>, 2006.
- 746 De Baar, H., de Jong, J., Bakker, D. et al. Importance of iron for plankton blooms and carbon dioxide drawdown in the
747 Southern Ocean. *Nature*, 373, 412–415 <https://doi.org/10.1038/373412a0>, 1995.
- 748 DeConto, R. & Pollard, D. Rapid Cenozoic glaciation of Antarctica induced by declining atmospheric CO₂. *Nature*, 421,
749 245–249. <https://doi.org/10.1038/nature01290>, 2003.
- 750 DeConto RM, Pollard D, Wilson PA, Palike H, Lear CH, Pagani M. Thresholds for Cenozoic bipolar glaciation.
751 doi:10.1038/nature07337, 2008.
- 752 Deppeler, S.L. and Davidson, A.T. Southern Ocean Phytoplankton in a Changing Climate. *Frontiers in Marine Science*,
753 4, <https://www.frontiersin.org/articles/10.3389/fmars.2017.00040>, 2017.
- 754 DeVries, T. The Ocean Carbon Cycle. *Annual Review of Environment and Resources*, 47, pp. 317-341,
755 <http://dx.doi.org/10.1146/annurev-environ-120920-111307>, 2022.
- 756 Diester-Haass, L. Late Eocene-Oligocene sedimentation in the Antarctic Ocean, Atlantic Sector (Maud Rise, ODP leg
757 113, Site 689), Development of surface and bottom water circulation, in *The Antarctic Paleoenvironment: A
758 Perspective on Global Change, Part 1, Antarct. Res. Ser.*, vol. 56, edited by J. P. Kennett, and D. A. Warnke, pp. 185–
759 202, AGU, Washington, D. C, 1992.
- 760 Diester-Haass, L. Middle Eocene to early Oligocene Paleooceanography of the Antarctic Ocean (Maud Rise, ODP Leg
761 113, Site 689): change from a low to a high productivity ocean. *Paleogeography, Paleoclimatology, Paleoecology*,
762 113, 311-334. [https://doi.org/10.1016/0031-0182\(95\)00067-V](https://doi.org/10.1016/0031-0182(95)00067-V), 1995.
- 763 Diester-Haass, L. Late Eocene-Oligocene paleoceanography in the southern Indian Ocean (ODP Site 744). *Marine
764 Geology*, 130, 99-119, 1996.
- 765 Diester-Haass, L & Zahn, R. Eocene-Oligocene transition in the Southern Ocean: History of water mass circulation and
766 biological productivity, *Geology*, 24, 163–166. 1996.
- 767 Diester-Haass, L & Zahn, R. Paleoproductivity increase at the Eocene-Oligocene climatic transition: ODP/DSDP Sites
768 763 and 592. *Paleogeography, Paleoclimatology, Paleoecology*, 172, 153-170. [https://doi.org/10.1016/S0031-0182\(01\)00280-2](https://doi.org/10.1016/S0031-0182(01)00280-2), 2001.
- 769 Diester-Haass, L. & Zachos, J. The Eocene-Oligocene transition in the Equatorial Atlantic (ODP Site 925);
770 paleoproductivity increase and positive d13C excursion. In Prothero, D.R; Ivany, L. C; Nesbitt, E. A. (eds) *From
771 greenhouse to icehouse; the marine Eocene-Oligocene transition*, *Columbia University Press*, New York, NY, United
772 States (USA), 2003.
- 773
774

- 775 Diester-Haass, L., & Faul, K. Paleoproductivity reconstructions for the Paleogene Southern Ocean: A direct comparison
776 of geochemical and micropaleontological proxies. *Paleoceanography and Paleoclimatology*, 34(1), 79– 97.
777 <https://doi.org/10.1029/2018PA003384>, 2019.
- 778 Doria, G., Royer, D. L., Wolfe, A. P., Fox, A., Westgate, J. A., & Beerling, D. J. Declining atmospheric CO₂ during the
779 late Middle Eocene climate transition. *American Journal of Science*, 311(1), 63-75.
780 <https://doi.org/10.2475/01.2011.03>, 2011.
- 781 Douglas, P.M.J., Affek, H.P., Ivany, L.C., Houben, A.J.P., Sijp, W.P., Sluijs, A., Schouten, S., Pagani, M. Pronounced
782 zonal heterogeneity in Eocene southern high-latitude sea surface temperatures. *PNAS*, 111 (18) 6582-6587
783 <https://doi.org/10.1073/pnas.1321441111>, 2014.
- 784 Dutkiewicz, A., Müller, R.D. The carbonate compensation depth in the South Atlantic Ocean since the Late Cretaceous.
785 *Geology*, 49 (7): 873–878. <https://doi.org/10.1130/G48404.1>, 2021.
- 786 Dymond, J., Suess, E. and Lyle, M. Barium in Deep-Sea Sediment: A Geochemical Proxy for Paleoproductivity.
787 *Paleoceanography and Paloclimatology*, 7(2), 163-181. <https://doi.org/10.1029/92PA00181>, 1992.
- 788 Egan, K.E., Rickaby, R.E.M., Hendry, K.R., Halliday, A.N. Opening the gateways for diatoms primes Earth for
789 Antarctic glaciation. *Earth Planetary Science Letters* 375, 34–43. <https://doi.org/10.1016/J.EPSL.2013.04.030> ,
790 2013
- 791 Ekart, D. D. A 400 million year carbon isotope record of pedogenic carbonate; implications for paleoatmospheric
792 carbon dioxide. *American Journal of Science*, 299(10), 805-827. <https://doi.org/10.2475/ajs.299.10.805>, 1999.
- 793 Elsworth, G., Galbraith, E., Halverson, G. et al. Enhanced weathering and CO₂ drawdown caused by latest Eocene
794 strengthening of the Atlantic meridional overturning circulation. *Nature Geoscience*, 10, 213–216.
795 <https://doi.org/10.1038/ngeo2888>, 2017.
- 796 Erdei, B., Utescher, T., Hably, L., Roth-Nebelsick, A., & Grein, M. Early Oligocene Continental Climate of the
797 Palaeogene Basin (Hungary and Slovenia) and the Surrounding Area. *Turkish Journal of Earth Sciences*, 21, 153-
798 186. <https://doi.org/10.3906/yer-1005-29>, 2012.
- 799 Faul K. L., Delaney, M. L. A comparison of early Paleogene export productivity and organic carbon burial flux for
800 Maud Rise, Weddell Sea, and Kerguelen Plateau, south Indian Ocean. *Paleoceanography*, v.25, 3214, 2010.
- 801 Florindo, F. and Roberts, A. P. Eocene-Oligocene magnetobiochronology of ODP Sites 689 and 690, Maud Rise,
802 Weddell Sea, Antarctica. *Geological Society of America Bulletin*, 117(1), 46–. doi:10.1130/b25541.1, 2005
- 803 Galeotti, S., Coccioni, R., Gersonde, R. Middle Eocene–Early Pliocene Subantarctic planktic foraminiferal
804 biostratigraphy of Site 1090, Agulhas Ridge, Marine Micropaleontology, 45, 3–4, 357-381,
805 [https://doi.org/10.1016/S0377-8398\(02\)00035-X](https://doi.org/10.1016/S0377-8398(02)00035-X), 2002. Gasson, E., Lunt, D. J., Deconto, R., Goldner, A.,
806 Heinemann, M., Huber, M., Legrande, A. N., Pollard, D., Sagoo, N., Siddall, M., Winguth, A., and Valdes, P. J.:
807 Uncertainties in the modelled CO₂ threshold for Antarctic glaciation. *Climate of the Past*, 10, 451-466,
808 2014. Gersonde, R., Hodell, B.A., Blum, P., and Shipboard Scientific Party. Leg 177 summary, Proc. Ocean Drill
809 Program, Initial Rep., 177, 1–67, 1999.
- 810 Glass, B.P., Hall, C.M., and York, D. 40Ar/39Ar laser probe dating of North American tektite fragments from Barbados
811 and the age of the Eocene-Oligocene boundary: *Chemical Geology*, v. 59, p. 181–186., 1996.
- 812 Goldner, A., Herold, N. and Huber, M. Antarctic glaciation caused ocean circulation changes at the Eocene-Oligocene
813 transition, *Nature*, 511(7511), 574–577, doi:10.1038/nature13597, 2014.
- 814 Gradstein, F. M., Ogg, J. G., Schmitz, M., & Ogg, G. The Geological Time Scale 2012 (pp. 1176). Oxford, UK:
815 Elsevier, 2012.
- 816 Griffith, E. M., Thomas, E., Lewis, A. R., Penman, D. E., Westerhold, T., and Winguth, A. M.: Benthic-Pelagic
817 Decoupling: The Marine Biological Carbon Pump During Eocene Hyperthermals. *Paleoceanography and*
818 *Paleoclimatology*, 36, <https://doi.org/10.1029/2020PA004053>, 2021.
- 819 Grein, M., Oehm, C., Konrad, W., Utescher, T., Kunzmann, L., and Roth-Nebelsick, A.: Atmospheric CO₂ from the late
820 Oligocene to early Miocene based on photosynthesis data and fossil leaf characteristics, *Palaeogeography,*
821 *Palaeoclimatology, Palaeoecology*, 374, 41–51, <https://doi.org/10.1016/j.palaeo.2012.12.025>, 2013.
- 822 Henderiks, J., & Pagani, M. Coccolithophore cell size and the Paleogene decline in atmospheric CO₂. *Earth and*
823 *Planetary Science Letters*, 269(3), 576–584. <https://doi.org/10.1016/j.epsl.2008.03.016>, 2008.
- 824 Henehan, M.; Edgar, K.M.; Foster, G.L., Penman, D.E.; Hull, P.M.; Greenop, R.; Anagnostou, E.; Pearson, P.N.
825 Revisiting the Middle Eocene Climatic Optimum “Carbon Cycle Conundrum” with New Estimates of Atmospheric
826 pCO₂ from Boron Isotopes. *Paleoceanography and Paleoclimatology*. 35(6). <https://doi.org/10.1029/2019PA003713>,
827 2020.
- 828 Hill, D. J., Haywood, A. M., Valdes, P. J., Francis, J. E., Lunt, D. J., Wade, B. S., and Bowman, V. C.: Paleogeographic
829 controls on the onset of the Antarctic circumpolar current, *Geophysical Research Letters*, 40, 5199-5204, 2013.
- 830 Houben, A.J.P., van Mourik, C.A., Montanari, A., Coccioni, R., Brinkhuis, H. The Eocene–Oligocene transition:
831 Changes in sea level, temperature or both? *Palaeogeography, Palaeoclimatology, Palaeoecology*. 335–336, p 75-83
832 <https://doi.org/10.1016/j.palaeo.2011.04.008>, 2012.

- 833 Houben, A. J. P., Bijl, P. K., Sluijs, A., Schouten, S., and Brinkhuis, H.: Late Eocene Southern Ocean cooling and
834 invigoration of circulation preconditioned Antarctica for full scale glaciation, *Geochemistry, Geophysics,*
835 *Geosystems*, 20, <https://doi.org/10.1029/2019GC008182>, 2019.
- 836 Huber, B.T. and Quilleyere, F. Revised Paleogene Planktonic Foraminiferal biozonation for the Austral realm. *Journal*
837 *of Foraminiferal Research*, 35(4), 299-314., 2005.
- 838 Huber, M., Brinkhuis, H., Stickley, C.E., Döös, K., Sluijs, A., Warner, J., Schellenberg, S.A. and Williams, G.L. Eocene
839 circulation of the Southern Ocean: Was Antarctica kept warm by subtropical waters? *Paleoceanography*, 19,
840 doi:10.1029/2004PA001014, 2004.
- 841 Huber, M. and Nof, D. The ocean circulation in the southern hemisphere and its climatic impacts in the Eocene.
842 *Palaeogeography, Palaeoclimatology, Palaeoecology*, 231, 9-28, <https://doi.org/10.1016/j.palaeo.2005.07.037>
843 2006.
- 844 Huck, C. E., van de Flierdt, T., Bohaty, S. M. and Hammond, S. J. Antarctic climate, Southern Ocean circulation
845 patterns, and deep-water formation during the Eocene. *Paleoceanography*, 32, 674– 691.
846 <https://doi.org/10.1002/2017PA003135>, 2017.
- 847 Hutchinson, D.K., Coxall, H.K., Lunt, D.J., Steinthorsdottir, M., de Boer, A.M. et al. The Eocene-Oligocene transition:
848 A review of marine and terrestrial proxy data, models and model-data comparisons. *Climate of the Past*, 17(1), 269-
849 315, 2021.
- 850 Inglis, G. N., Farnsworth, A., Lunt, D., Foster, G. L., Hollis, C. J., Pagani, M., Jardine, P. E., Pearson, P. N., Markwick,
851 P., Galsworthy, A. M. J., Raynham, L., Taylor, K. W. R. and Pancost, R. D. Descent toward the Icehouse: Eocene sea
852 surface cooling inferred from GDGT distributions, *Paleoceanography*, 30(7), 1000–1020,
853 doi:10.1002/2014PA002723, 2015.
- 854 Inokuchi, H; Heider, F. Paleolatitude of the southern Kerguelen Plateau inferred from the paleomagnetic study of late
855 Cretaceous basalts. In: Wise, SW; Schlich, R; et al. (eds.), Proceedings of the Ocean Drilling Program, Scientific
856 Results, College Station, TX (Ocean Drilling Program), 120, 89-96,
857 <https://doi.org/10.2973/odp.proc.sr.120.129.1992>
- 858 IPCC. Climate Change 2021: The Physical Science Basis. Working Group I Contribution to the Sixth Assessment
859 Report of the Intergovernmental Panel on Climate Change. *Cambridge University Press*, Cambridge, United
860 Kingdom and New York, NY, USA, 2391pp, 2021.
- 861 Katz, M.E., Cramer, B.S., Toggweiler, J.R., Esmay, G., Liu, C., Miller, K.G., Rosenthal, Y., Wade, B.S., Wright J.D.
862 Impact of Antarctic Circumpolar Current Development on Late Paleogene Ocean Structure. *Science*, 332, 1076-
863 1079, DOI: 10.1126/science.1202122, 2011.
- 864 Kennet, J.P. Cenozoic evolution of Antarctic glaciation, the circum-Antarctic Ocean, and their impact on global
865 paleoceanography. *Journal of Geophysical Research*, 82, 3843-3860,
866 <https://doi.org/10.1029/JC082i027p03843>,1977.
- 867 Kennett, J.P. and Stott, L.D. Proteus and Proto-Oceanus: ancestral Paleogene oceans as revealed from antarctic stable
868 isotopic results: ODP Leg 113. In: Leg 113. ODP Sci. Res., pp. 865-880, 1990.
- 869 Kim J.H., Crosta, X., Michel, E., Schouten, S., Duprat, J., Damsté, J.S.S. Impact of lateral transport on organic proxies
870 in the Southern Ocean, *Quaternary Research*, 71(2), 246-250. <https://doi.org/10.1016/j.yqres.2008.10.005>, 2009.
- 871 Kim, Yong Sun, Orsi, Alejandro H. On the Variability of Antarctic Circumpolar Current Fronts Inferred from 1992–
872 2011 Altimetry. *Journal of Physical Oceanography*, 3054–3071. <https://doi.org/10.1175/JPO-D-13-0217.1>, 2014.
- 873 Kohn, M. J., Strömberg, C. A., Madden, R. H., Dunn, R. E., Evans, S., Palacios, A., & Carlini, A. A. Quasi-static
874 Eocene–Oligocene climate in Patagonia promotes slow faunal evolution and mid-Cenozoic global cooling.
875 *Palaeogeography, Palaeoclimatology, Palaeoecology*, 435, 24-37. <https://doi.org/10.1016/j.palaeo.2015.05.028>,
876 2015.
- 877 Kuhlbrodt, T., Griesel, A., Montoya, M., Levermann, A., Hofmann, M., Rahmstorf, S. On the driving processes of the
878 Atlantic meridional overturning circulation. *Reviews of Geophysics*, 45, RG2001, doi:10.1029/2004RG000166, 2007.
- 879 Kürschner, W. M., Kvaček, Z., & Dilcher, D. L. The impact of Miocene atmospheric carbon dioxide fluctuations on
880 climate and the evolution of terrestrial ecosystems. *Proceedings of the National Academy of Sciences*, 105(2), 449-
881 453. <https://doi.org/10.1073/pnas.0708588105>, 2008.
- 882 Ladant, J.-B., Donnadieu, Y. and Dumas, C. Links between CO₂, glaciation and water flow: reconciling the Cenozoic
883 history 1680 of the Antarctic Circumpolar Current, *Climate of the Past*, 10(6), 1957–1966, doi:10.5194/cp-10-1957-
884 2014, 2014.
- 885 Lauretano, V., Kennedy-Asser, A.T., Korasidis, V.A., Wallace, M.W., Valdes, P.J., Lunt, D.J., Pancost, R.D. and Naafs,
886 B.D.A. Eocene to Oligocene terrestrial Southern Hemisphere cooling caused by declining pCO₂. *Nature Geoscience*
887 14, 659–664. <https://doi.org/10.1038/s41561-021-00788-z>, 2021.
- 888 Lazarus, D. and Caulet J.P. Cenozoic Southern Ocean reconstructions from sedimentologic, radiolarian, and other
889 microfossil data. In: J.P. Kennett and D.A. Warnke, Eds., The Antarctic Paleoenvironment: A perspective on global
890 change. Pt. 2. *Antarctic Research Series*, 60: 145-174, 1994.

891 Li, Z., Lozier, M.S., Cassar, N. Linking Southern Ocean Mixed Layer Dynamics to Net Community Production on
892 Various Timescales. *JGR Oceans*, 126. <https://doi.org/10.1029/2021JC017537>, 2021.

893 Liu, Z., M., Pagani, D., Zinniker, R., DeConto, M., Huber, H., Brinkhuis, S. R., Shah, R. M. Leckie, and Pearson, A.
894 Global cooling during the Eocene – Oligocene climate transition, *Science*, 323, 1187–1190, 2009.

895 Livermore, R., Nankivell, Eagles, G. and Morris, P. Paleogene opening of Drake Passage, *Earth Planetary Science
896 Letters*, 236, 459–470, 2005.

897 Livermore, R., Hillenbrand, C., Meredith, M., and Eagles, G. Drake Passage and Cenozoic climate: an open and shut
898 case?, *Geochemistry, Geophysics, Geosystems*, 8, Q01005, <https://doi.org/10.1029/2005GC001224>, 2007.

899 Mackensen, A., and Ehrmann, W.U. Middle Eocene through Early Oligocene climate history and paleoceanography in
900 the Southern Ocean: Stable oxygen and carbon isotopes from ODP Sites on Maud Rise and Kerguelen Plateau,
901 *Marine Geology*, 108, 1–27, [https://doi.org/10.1016/0025-3227\(92\)90210-9](https://doi.org/10.1016/0025-3227(92)90210-9), 1992.

902 Marino, M. and Flores, J.A. Middle Eocene to early Oligocene calcareous nannofossil stratigraphy at Leg 177 Site
903 1090, *Marine Micropaleontology*, 45, 383–398, 2002.

904 Martin, E.E. and Haley, B.A. Fossil fish teeth as proxies for seawater Sr and Nd isotopes. *Geochimica et Cosmochimica
905 Acta*, 64 (5), 835-847, doi:10.1016/S0016-7037(99)00376-2, 2000.

906 Martin, E.E. and Scher, H.D. Preservation of seawater Sr and Nd isotopes in fossil fish teeth: bad news and good news.
907 *Earth and Planetary Science Letters*, 220(1-2), 25-39, [https://doi.org/10.1016/S0012-821X\(04\)00030-5](https://doi.org/10.1016/S0012-821X(04)00030-5), 2004.

908 Mikolajewicz, U., Maier-Reimer, E., Crowley, T. J. and Kim, K.-Y. Effect of Drake and Panamanian Gateways on the
909 circulation of an ocean model, *Paleoceanography*, 8(4), 409–426, doi:10.1029/93PA00893, 1993.

910 Miller, K.G. Janecek, T.R., Katz, M.E., Keil, D.J. Abyssal circulation and benthic foraminiferal changes near the
911 Paleocene/Eocene boundary. *Paleoceanography*, 2(6), 741-761, <https://doi.org/10.1029/PA002i006p00741>, 1987.

912 Moore, J. K., M. R. Abbott, J. G. Richman, W. O. Smith, T. J. Cowles, K. H. Coale, W. D. Gardner, and R. T. Barber.
913 SeaWiFS satellite ocean color data from the Southern Ocean, *Geophysical Research Letters*, 26, 1465–1468, 1999.

914 Muza, J.P., Williams, D.F., Wise, S.W. Paleogene oxygen record for Deep Sea Drilling Project Sites 511 and 512,
915 subantarctic South Atlantic Ocean: Paleotemperatures, paleoceanographic changes, and the Eocene/Oligocene
916 boundary event. In: Ludwig, WJ; Krasheninnikov, VA; et al. (Eds.), Initial Reports of the Deep-Sea Drilling Project
917 (U.S. Govt. Printing Office), 71, 409-422, <https://doi.org/10.2973/dsdp.proc.71.117.1983>, 1983.

918 Najjar, R.G., Nong, G.T., Seidov, D., Peterson, W.H. Modelling geographic impacts on early Eocene ocean temperature,
919 *Geophysical Research Letters*, 29 (15), 401-404. <https://doi.org/10.1029/2001GL014438>, 2002.

920 Nelson, D.M. & Smith, W. Sverdrup revisited: Critical depths, maximum chlorophyll levels, and the control of Southern
921 Ocean productivity by the irradiance-mixing regime. *Limnology and Oceanography*. 36, 1650–1661.
922 <https://doi.org/10.4319/lo.1991.36.8.1650>, 1991.

923 Nielsen, E.B., Anderson, L.D., Delaney, M.L. Paleoproductivity, nutrient burial, climate change and the carbon cycle in
924 the western equatorial Atlantic across the Eocene/Oligocene boundary. *Paleoceanography*, v 18, n. 3, 1057,
925 doi:10.1029/2002PA000804, 2003.

926 Nooteboom, P. D., Baatsen, M., Bijl, P. K., Kliphuis, M. A., van Sebille, E., Sluijs, A., Dijkstra, H. A., and von der
927 Heydt, A. S.: Improved Model-Data Agreement With Strongly Eddying Ocean Simulations in the Middle-Late
928 Eocene. *Paleoceanography and Paleoclimatology*, 37, 10.1029/2021PA004405, 2022.

929 O'Brien, C. L., Huber, M., Thomas, E., Pagani, M., Super, J. R., Elder, L. E., Hull, P. M. The enigma of Oligocene
930 climate and global surface temperature evolution. *Proceedings of the National Academy of Sciences* Oct 2020, 117
931 (41) 25302-25309; doiDOI:10.1073/pnas.2003914117, 2020.

932 Olivarez Lyle, A., and M. W. Lyle. Missing organic carbon in Eocene marine sediments: Is metabolism the biological
933 feedback that maintains end-member climates?, *Paleoceanography*, 21, PA2007, doi:10.1029/2005PA001230, 2006.

934 Orsi, A.H., Whitworth, T., Nowlin, W.D. On the meridional extent and fronts of the Antarctic Circumpolar Current,
935 Deep Sea Research Part I: *Oceanographic Research Papers*, v 42, 5, 641-673, [https://doi.org/10.1016/0967-
936 0637\(95\)00021-W](https://doi.org/10.1016/0967-

936 0637(95)00021-W), 1995.

937 Pagani, M. Late Miocene Atmospheric CO₂ Concentrations and the Expansion of C4 Grasses. *Science*, 285(5429), 876-
938 879. <https://doi.org/10.1126/science.285.5429.876>, 1999.

939 Pagani, M., Arthur, M. A., & Freeman, K. H. Miocene evolution of atmospheric carbon dioxide. *Paleoceanography*,
940 14(3), 273-292. <https://doi.org/10.1029/1999pa900006>, 1999.

941 Pagani, M., Zachos, J. C., Freeman, K. H., Tipler, B., and Bohaty, S. Marked decline in atmospheric carbon dioxide
942 concentrations during the Paleogene. *Science*, 309 600–603. DOI: 10.1126/science.111006, 2005

943 Pagani, M., Huber, M., Liu, Z., Bohaty, S.M., Henderiks, J., Sijp, W., Krishnan, S. & DeConto, R.M. The role of carbon
944 dioxide during the onset of Antarctic glaciation. *Science*, 334, 1261-1264. DOI: 10.1126/science.1203909, 2011.

945 Pälike, H., Lyle, M.W., Nishi, H., Raffi, I., Ridgwell, A., Gamage, K., Klaus, A., Acton, G., Anderson, L., Backman, J.,
946 Baldauf, J., Beltran, C., Bohaty, S.M., Bown, P., Busch, W., Channell, J.E.T., Chun, C.O.J., Delaney, M., Dewangan,
947 P., Dunkley Jones, T., Edgar, K.M., Evans, H., Fitch, P., Foster, G.L., Gussone, N., Hasegawa, H., Hathorne, E.C.,
948 Hayashi, H., Herrle, J.O., Holbourn, A., Hovan, S., Hyeong, K., Iijima, K., Ito, T., Kamikuri, S., Kimoto, K.,
949 Kuroda, J., Leon-Rodriguez, L., Malinverno, A., Moore, T.C., Murphy, B.H., Murphy, D.P., Nakamura, H., Ogane,

950 K., Ohneiser, C., Richter, C., Robinson, R., Rohling, E.J., Romero, O., Sawada, K., Scher, H., Schneider, L., Sluijs,
 951 A., Takata, H., Tian, J., Tsujimoto, A., Wade, B.S., Westerhold, T., Wilkens, R., Williams, T., Wilson, P.A.,
 952 Yamamoto, Y., Yamamoto, S., Yamazaki, T., Zeebe, R.E. A Cenozoic record of the equatorial Pacific carbonate
 953 compensation depth, *Nature*, 488 (7413), 609-615, doi:10.1038/nature11360, 2012.
 954 Palter, J. B., Sarmiento, J. L., Marinov, I. & Gruber, N. In: Chemical Oceanography of Frontal Zones (ed. Belkin, I. M.)
 955 https://doi.org/10.1007/698_2013_241 (Springer), 2013.
 956 Pearson, P., Foster, G. and Wade, B. Atmospheric carbon dioxide through the Eocene–Oligocene climate transition.
 957 *Nature*, 461, 1110–1113. <https://doi.org/10.1038/nature08447>, 2009.
 958 Persico, D., and Villa, G. High-resolution calcareous nannofossil biostratigraphy and palaeoecology from Eocene-
 959 Oligocene sediments, Maud Rise, Weddell Sea, and Kerguelen Plateau, Antarctica: University of Parma, Italy,
 960 Abstract 9th International Nannoplankton Association Conference, 8th–14th September 2002.
 961 Persico, D., and Villa, G. Eocene-Oligocene calcareous nannofossils from Maud Rise and Kerguelen Plateau
 962 (Antarctica): Palaeoecological and palaeoceanographic implications: *Marine Micropaleontology*, v. 52, p. 153–179,
 963 doi: 10.1016/j.marmicro.2004.05.002, 2004.
 964 Pfuhl, H. A. & McCave, I. N. Evidence for late Oligocene establishment of the Antarctic Circumpolar Current. *Earth
 965 and Planetary Science Letters*, 235, 715–728, 2005.
 966 Piepgras D.J., Wasserburg G.J. Isotopic composition of neodymium in waters from the drake passage. *Science* Jul
 967 16;217(4556):207-14. doi: 10.1126/science.217.4556.207, 1982.
 968 Prothero, D.R. & Berggren, W.A. Eocene-Oligocene Climatic and Biotic Evolution. *Princeton University Press*,
 969 Princeton, NJ, 1992.
 970 Pusz, A. E., Thunell, R.C. and Miller, K.G. Deep water temperature, carbonate ion, and ice volume changes across the
 971 Eocene-Oligocene climate transition, *Paleoceanography*, 26, PA2205, doi:10.1029/2010PA001950, 2011.
 972 Rea, D. K. and Lyle, M. W.: Paleogene calcite compensation depth in the eastern subtropical Pacific: Answers and
 973 questions. *Paleoceanography*, 20, PA1012, doi:10.1029/2004PA001064, 2005.
 974 Reichgelt, T., D'Andrea, W. J., & Fox, B. R. Abrupt plant physiological changes in southern New Zealand at the
 975 termination of the Mi-1 event reflect shifts in hydroclimate and pCO₂. *Earth and Planetary Science Letters*, 455,
 976 115-124. <https://doi.org/10.1016/j.epsl.2016.09.026>, 2016
 977 Renaudie, J., Lazarus, D. and Diver, P. NSB (Neptune Sandbox Berlin): An expanded and improved database of marine
 978 planktonic microfossil data and deep-sea stratigraphy. *Palaeontologia Electronica*, 23(1):a11
 979 <https://doi.org/10.26879/1032>, 2020.
 980 Retallack, G. J.: Refining a pedogenic-carbonate CO₂ paleobarometer to quantify a middle Miocene greenhouse spike,
 981 *Palaeogeography Palaeoclimatology, Palaeoecology*, 281, 57–65, 2009.
 982 Rintoul, S.R., Hughes, C.W., Olbers, D. Chapter 4.6 The antarctic circumpolar current system, Editor(s): Gerold Siedler,
 983 John Church, John Gould, *International Geophysics, Academic Press*, v.77, 271-XXXVI, 2001.
 984 Robert, C., Diester Haass, L. and Chamley, H. Late Eocene Oligocene oceanographic development at southern high
 985 latitudes, from terrigenous and biogenic particles: A comparison of Kerguelen Plateau and Maud Rise, ODP Sites
 986 744 and 689, *Marine Geology*, 191, 37–54, doi:10.1016/S0025-3227(02)00508-X, 2002.
 987 Roberts, A.P., Bicknell, S.J., Byatt, J., Bohaty, S.M., Florindo, F., and Harwood, D.M. Magnetostratigraphic calibration
 988 of Southern Ocean diatom datums from the Eocene-Oligocene of Kerguelen Plateau (Ocean Drilling Program Sites
 989 744 and 748): *Palaeogeography, Palaeoclimatology, Palaeoecology*, v. 198, p. 145–168, doi: 10.1016/S0031-
 990 0182(03)00397-3, 2003.
 991 Roberts, N.L., Piotrowski, A.M., McManus, J.F., Keigwin, L.D. Synchronous deglacial overturning and water mass
 992 source changes. *Science* 84 327, 75e78. <https://doi.org/10.1126/science.1178068>, 2010.
 993 Roth-Nebelsick, A., Utescher, T., Mosbrugger, V., Diester-Haass, L., and Walther, H.: Changes in atmospheric CO₂
 994 concentrations and climate from the Late Eocene to Early Miocene: palaeobotanical reconstruction based on fossil
 995 floras from Saxony, Germany, *Palaeogeography Palaeoclimatology Palaeoecology*, 205, 43–67,
 996 <https://doi.org/10.1016/j.palaeo.2003.11.014>, 2004.
 997 Roth-Nebelsick, A., Grein, M., Utescher, T., and Konrad, W.: Stomatal pore length change in leaves of
 998 *Eotrigonobalanus furcinervis* (Fagaceae) from the Late Eocene to the Latest Oligocene and its impact on gas
 999 exchange and CO₂ reconstruction, *Rev. Palaeobot. Palynol.*, 174, 106–112,
 1000 <https://doi.org/10.1016/j.revpalbo.2012.01.001>, 2012.
 1001 Roth-Nebelsick, A., Oehm, C., Grein, M., Utescher, T., Kunzmann, L., Friedrich, J.-P., & Konrad, W. Stomatal density
 1002 and index data of *Platanus neptuni* leaf fossils and their evaluation as a CO₂ proxy for the Oligocene. *Review of
 1003 Palaeobotany and Palynology*, 206,1–9. <https://doi.org/10.1016/j.revpalbo.2014.03.001>, 2014.
 1004 Salamy, K.A & Zachos, J.C. Latest Eocene-Early Oligocene climate change and Southern Ocean fertility: inferences
 1005 from sediment accumulation and stable isotope data. *Paleogeography, Paleoclimatology, Paleoecology*, 145, 61-77.
 1006 [https://doi.org/10.1016/S0031-0182\(98\)00093-5](https://doi.org/10.1016/S0031-0182(98)00093-5), 1992.
 1007 Sarkar, S., Basak, C., Frank, M. Late Eocene onset of the Proto-Antarctic Circumpolar Current. *Science Reports*, 9,
 1008 10125, 2019.

- 1009 Sarmiento, J.L., Gruber, N., Brzezinski, M.A., Dunne, J.P. High-latitude controls of thermocline nutrients and low
1010 latitude biological productivity. *Nature* 247, 56–60, 2004.
- 1011 Sauermilch, I., Whittaker, J.M., Klocker, A. et al. Gateway-driven weakening of ocean gyres leads to Southern Ocean
1012 cooling. *Nature Communications* 12, 6465. <https://doi.org/10.1038/s41467-021-26658-1>, 2021.
- 1013 Scher, H.D. and Martin, E.E. Circulation in the Southern Ocean during the Paleogene inferred from neodymium
1014 isotopes. *Earth Planet. Sci. Lett.* 228, 391–405. <https://doi.org/10.1016/J.EPSL.2004.10.016>, 2004.
- 1015 Scher, H. D. and Martin, E. E. Timing and climatic consequences of the opening of Drake Passage. *Science*, 312, 428–
1016 430. DOI: 10.1126/science.1120044, 2006.
- 1017 Scher H. D., Delaney M. L. Breaking the glass ceiling for high resolution Nd isotope records in early Cenozoic
1018 paleoceanography. *Chem. Geol.* 269, 329–338. doi: 10.1016/j.chemgeo.2009.10.007, 2010.
- 1019 Scher, H.D., Bohaty, S.M., Zachos, J.C., Delaney, M.L. Two-stepping into the icehouse: East Antarctic weathering
1020 during progressive ice-sheet expansion at the Eocene–Oligocene transition. *Geology*, 2011; 39 (4): 383–386.
1021 doi:<https://doi.org/10.1130/G31726.1>, 2011
- 1022 Scher, H.D., Bohaty, S.M., Smith, B.W., Munn, G.H. Isotopic interrogation of a suspected late Eocene glaciation.
1023 *Paleoceanography* 29, 628–644. <https://doi.org/10.1002/2014PA002648>, 2014.
- 1024 Scher, H., Whittaker, J., Williams, S. et al. Onset of Antarctic Circumpolar Current 30 million years ago as Tasmanian
1025 Gateway aligned with westerlies. *Nature* 523 580–583. <https://doi.org/10.1038/nature14598>, 2015.
- 1026 Schumacher, S. and Lazarus, D. Regional differences in pelagic productivity in the late Eocene to early Oligocene—a
1027 comparison of southern high latitudes and lower latitudes. *Paleogeography, Paleoclimatology, Paleocology*, 214,
1028 243-263. <https://doi.org/10.1016/j.palaeo.2004.06.018>, 2004.
- 1029 Seton, M., Müller, R., Zahirovic, S., Gaina, C., Torsvik, T., Shephard, G., Talsma, A., Gurnis, M., Turner, M., Maus, S.,
1030 and Chandler, M. Global continental and ocean basin reconstructions since 200Ma. *Earth-Science Reviews*,
1031 113:212-270. <https://doi.org/10.1016/j.earscirev.2012.03.002>, 2012.
- 1032 Shackleton, N.J. and Opdyke, N.D. Oxygen isotope and paleomagnetic stratigraphy of equatorial Pacific core V28-238:
1033 Oxygen isotope temperatures and ice volumes on a 105 year and 106 year scale. *Quat. Res.*, 3(1), 39-55,
1034 doi::10.1016/0033-5894(73)90052-5, 1973.
- 1035 Shackleton, N. J., and Kennett, P. Paleotemperature history of the Cenozoic and the initiation of Antarctic glaciation:
1036 Oxygen and carbon isotope analysis in DSDP Sites 277, 279 and 281, Initial Rep. Deep Sea Drill. Proj., 29, 881–
1037 884, 1975.
- 1038 Shackleton, N.J., Hall, M.A., Boersma, A. Oxygen and carbon isotope data from Leg 74 foraminifers. *Init. Rep. Deep*
1039 *Sea Drilling Proj.*, 74, pp. 599-612, 1984.
- 1040 Sigman, D. M. & Boyle, E. A. Glacial/interglacial variations in atmospheric carbon dioxide. *Nature*, 407, 859–869,
1041 2000.
- 1042 Sigman, D., Hain, M. & Haug, G. The polar ocean and glacial cycles in atmospheric CO₂ concentration. *Nature*, 466,
1043 47–55, <https://doi.org/10.1038/nature09149>, 2010.
- 1044 Sijp, W. P., England, M. H. and Toggweiler, J. R. Effect of Ocean Gateway Changes under Greenhouse Warmth,
1045 *Journal of Climate*, 22(24), 6639–6652, doi:10.1175/2009JCLI3003.1, 2009.
- 1046 Sijp, W. P., England, M.H., and Huber, M. Effect of the deepening of the Tasman Gateway on the global ocean.
1047 *Paleoceanography*, 26, doi:10.1029/2011PA002143, 2011.
- 1048 Sijp, W. P., von der Heydt, A. S., and Bijl, P. K.: Model simulations of early westward flow across the Tasman Gateway
1049 during the early Eocene, *Climate of the Past*, 12, 807–817, <https://doi.org/10.5194/cp-12-807-2016>, 2016.
- 1050 Sluijs, A., Zeebe, R. E., Bijl, P. K., & Bohaty, S. M. A middle Eocene carbon cycle conundrum. *Nature Geoscience*,
1051 6(6), 429–434. <https://doi.org/10.1038/ngeo1807>, 2013
- 1052 Sokolov, S., Rintoul, S.R. Circumpolar structure and distribution of the Antarctic Circumpolar Current fronts: 1. Mean
1053 circumpolar paths. *J. Geophys. Res.* 114, 2009.
- 1054 Srivastava, P., Patel, S., Singh, N., Jamir, T., Kumar, N., Aruche, M., & Patel, R. C. Early Oligocene paleosols of the
1055 Dagshai Formation, India: A record of the oldest tropical weathering in the Himalayan foreland. *Sedimentary*
1056 *Geology*, 294, 142-156. <https://doi.org/10.1016/j.sedgeo.2013.05.011>, 2013.
- 1057 Steinhorsdottir, M., Porter, A. S., Holohan, A., Kunzmann, L., Collinson, M., & McElwain, J. C. Fossil plant stomata
1058 indicate decreasing atmospheric CO₂ prior to the Eocene–Oligocene boundary. *Climate of the Past*, 12(2), 439-
1059 454. <https://doi.org/10.5194/cp-12-439-2016>, 2016.
- 1060 Stickley, C.E., Brinkhuis, H., Schellenberg, S.A., Sluijs, A., Röhl, U., Fuller, M., Grauert, M., Huber, M., Warnaar, J.,
1061 Williams, G.L. Timing and nature of the deepening of the Tasmanian Gateway. *Paleoceanography*, 19 (4).
1062 <https://doi.org/10.1029/2004PA001022>, 2004.
- 1063 Sun, B. N., Wang, Q. J., Konrad, W., Ma, F. J., Dong, J. L., & Wang, Z. X. Reconstruction of atmospheric CO₂ during
1064 the Oligocene based on leaf fossils from the Ningming Formation in Guangxi, China. *Palaeogeography,*
1065 *Palaeoclimatology, Palaeoecology*, 467, 5-15. <https://doi.org/10.1016/j.palaeo.2016.09.015>, 2017.
- 1066 Taylor, V. E., Westerhold, T., Bohaty, S.M., Backman, J., Dunkley Jones, T., Edgar, K. M., Egan, K. E., Lyle, M.,
1067 Pälike, H., Röhl, U., Zachos, J., Wilson, P. A. Transient Shoaling, Over-Deepening and Settling of the Calcite

1068 Compensation Depth at the Eocene-Oligocene Transition. *Paleoceanography and Paleoclimatology*, 38(6),
1069 <https://doi.org/10.1029/2022PA004493>, 2023

1070 The Cenozoic CO₂ Proxy Integration Project Consortium, (2023). Toward a Cenozoic History of Atmospheric CO₂.
1071 *Science* 382, eadi5177. doi:10.1126/science.adi5177

1072 Thole, L.M., Amsler, H.E., Moretti, S., Auderset, A., Gilgannon, J., Lippold, J., Vogel, H., Crosta, X., Mazaud, A.,
1073 Michel, E., Martínez-García, A., Jaccard, S.L. Glacial- Interglacial dust and export production records from the
1074 Southern Indian Ocean. *Earth and Planetary Science Letters* 525, <https://doi.org/10.1016/j.epsl.2019.115716>, 2019.

1075 Thomas, E. Late Cretaceous through Neogene deep-sea benthic foraminifera (Maud Rise, Weddell Sea, Antarctica).
1076 *Proc. Ocean Drill. Program Sci. Results* 113, 571–594, 1990.

1077 Toggweiler, J. R. and Samuels, B. Effect of Drake Passage on the global thermohaline circulation. *Deep-Sea Res. I* 42,
1078 477–500, 1995.

1079 Toumoulin, A., Donnadiou, Y., Ladant, J., Batenburg, S.J., Poblete, F. and Dupont-Nivet, G. (2020). Quantifying the
1080 Effect of the Drake Passage Opening on the Eocene Ocean. *Paleoceanography and Paleoclimatology*, 35(8)
1081 <https://doi.org/10.1029/2020PA003889>, 2000.

1082 Van Breedam, J., Huybrechts, P., Crucifix, M. Modelling evidence for late Eocene Antarctic glaciations, *Earth and*
1083 *Planetary Science Letters*, 586, 117532, ISSN 0012-821X, <https://doi.org/10.1016/j.epsl.2022.117532>, 2022.

1084 Villa, G., Fiorini, C., Persico, D., Roberts, A.P. Florindo, F. Middle Eocene to Late Oligocene Antarctic
1085 glaciation/deglaciation and Southern Ocean productivity. *Paleoceanography and Paloclimatology*, 29, 223-237.
1086 <https://doi.org/10.1002/2013PA002518>, 2014.

1087 Volk, T. and Hoffert, M. I.: Ocean Carbon Pumps: Analysis of Relative Strengths and Efficiencies in Ocean-Driven
1088 Atmospheric CO₂ Changes, in: *The Carbon Cycle and Atmospheric CO₂: Natural Variations Archean to Present*,
1089 edited by: Sundquist, E. T. and Broecker, W. S., AGU, 99–110, 1985.

1090 Vonhof, H.B., Smit, J., Brinkhuis, H., Montanari, A., and Nederbragt, A.J. Global cooling accelerated by early late
1091 Eocene impacts: *Geology*, v. 28, p. 687–690, doi: 10.1130/0091-7613(2000)0282.3.CO;2, 2000.

1092 Wei, W. Paleogene chronology of Southern Ocean drill holes: An update, in Kennett, J.P., and Warnke, D.A., eds., *The*
1093 *Antarctic paleoenvironment: A perspective on global change: Antarctic Research Series*, v. 56, p. 75–96, 1992.

1094 Wei, W., and Wise, S.W. Jr. Eocene-Oligocene calcareous nannofossil magnetobiochronology of the Southern Ocean:
1095 *Newsletters on Stratigraphy*, v. 26, p. 119–132, 1992.

1096 Westerhold, T., Marwan, N., Drury, A.J., Liebrand, D., Agnini, C., Anagnostou, E., Barnet, J.S.K., Bohaty, S.M.,
1097 Vleeschouwer, Florindo, F., Frederichs, T., Hodell, D.A., Holbourn, A.E., Kroon, D., Laurentano, V., Littler, K.,
1098 Lourens, L.J., Lyle, M., Pálike, H., Röhl, U., Tian, J., Wilkens, R.H., Wilson, P.A. and Zachos, J.C. An
1099 astronomically dated record of Earth's climate and its predictability over the last 66 million years. *Science*, 369,
1100 6509, 1383-1387. DOI: 10.1126/science.aba6853, 2020.

1101 Wright, N.M., Scher, H.D., Seton, M., Huck, C.E., Duggan, B.D. No change in Southern Ocean Circulation in the
1102 Indian Ocean from the Eocene through Late Oligocene. *Paleoceanography, Paleoclimatology*, 33, 152–167.
1103 <https://doi.org/10.1002/2017PA003238>, 2018.

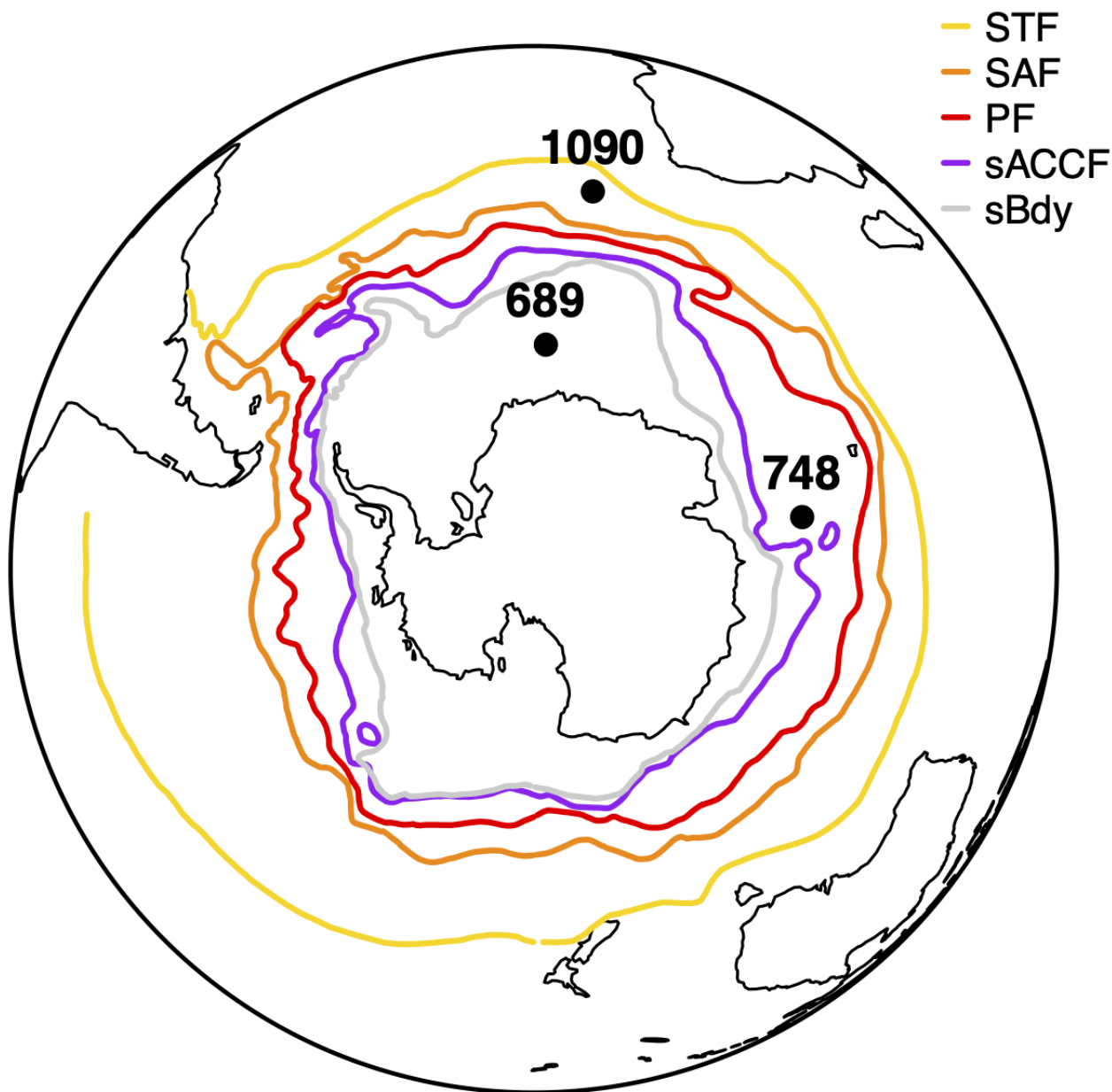
1104 Zachos, C. J., T. M. Quinn, and K. A. Salamy. High-resolution (104 years) deep-sea foraminiferal stable isotope records
1105 of the Eocene-Oligocene climate transition, *Paleoceanography*, 11, 251–266, 1996.

1106 Zachos, C. J., B. N. Opdyke, T. M. Quinn, C. E. Jones, and A. N. Halliday. Early Cenozoic glaciation, Antarctic
1107 weathering, and seawater 87Sr/86Sr: Is there a link? *Chem. Geol.*, 161, 165–180, 1999.

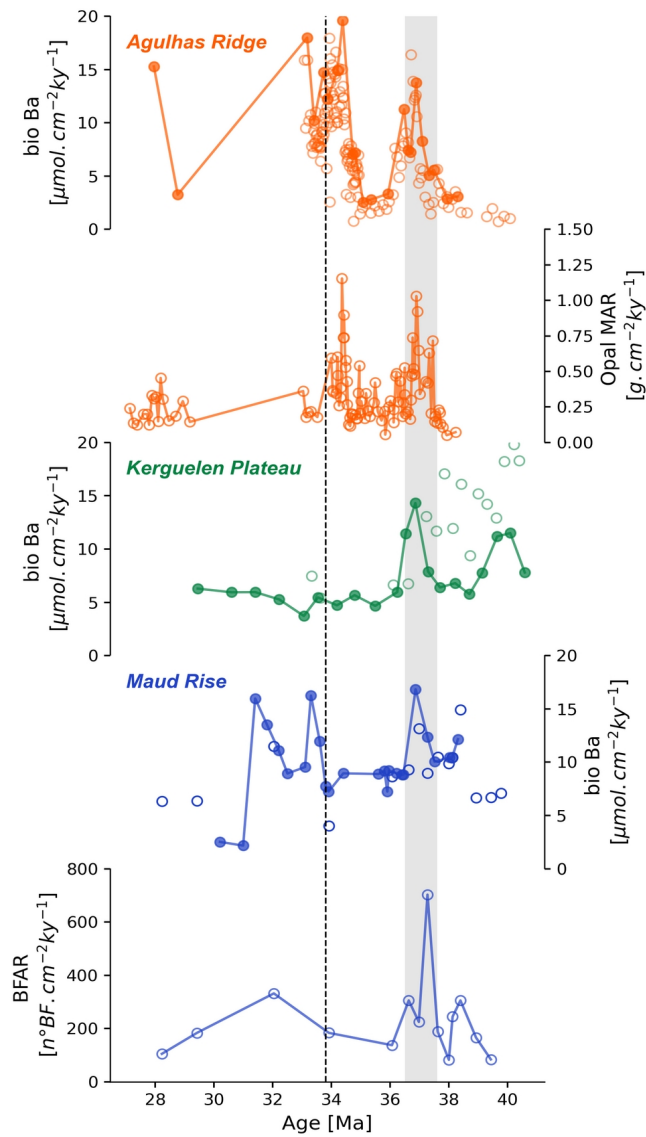
1108 Zachos, J., Pagani, M., Sloan, L., Thomas, E., Billups, K. Trends, rhythms and aberrations in global climate 65 Ma to
1109 present. *Science*, 292, 686-693. <https://doi.org/10.1126/science.1059412>, 2001.

1110 Zachos, J., Kump, L. Carbon cycle feedbacks and the initiation of Antarctic glaciation in the earliest Oligocene. *Global*
1111 *and Planetary Change*, 47 (1). 51-66 doi:10.1016/j.gloplacha.2005.01.001, 2005.

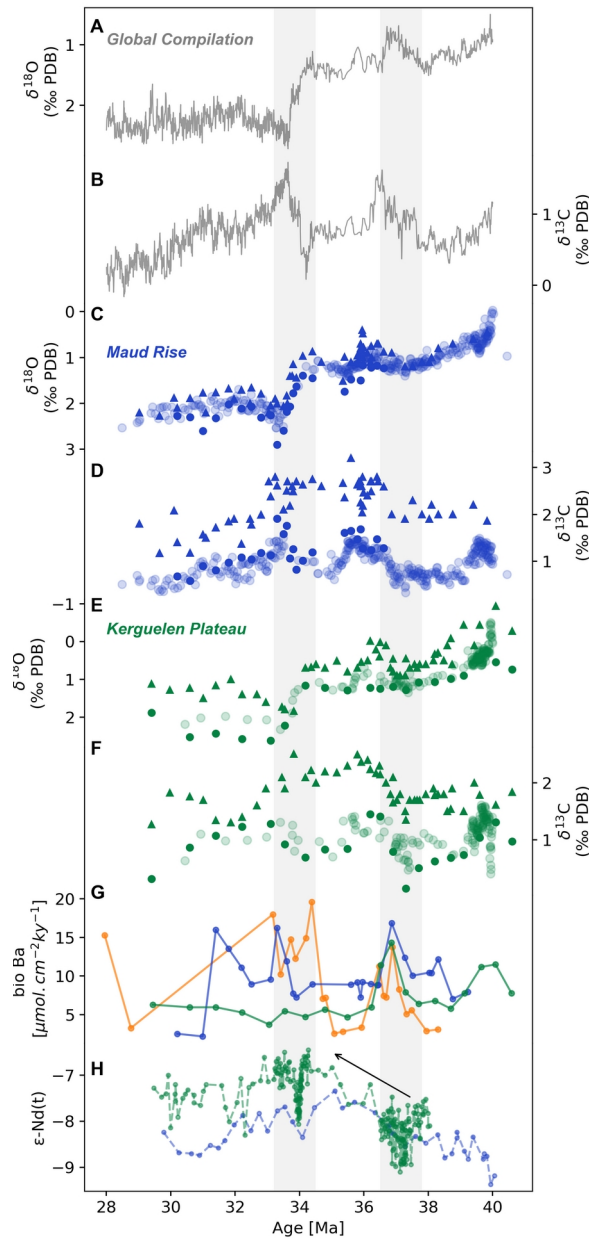
1112 Zhang, Y. G., Pagani, M., Liu, Z., Bohaty, S. M., and DeConto, R. A 40-million-year history of atmospheric CO₂.
1113 *Philosophical Transactions of the Royal Society A*, v. 371, <https://doi.org/10.1098/rsta.2013.0096>, 2013.



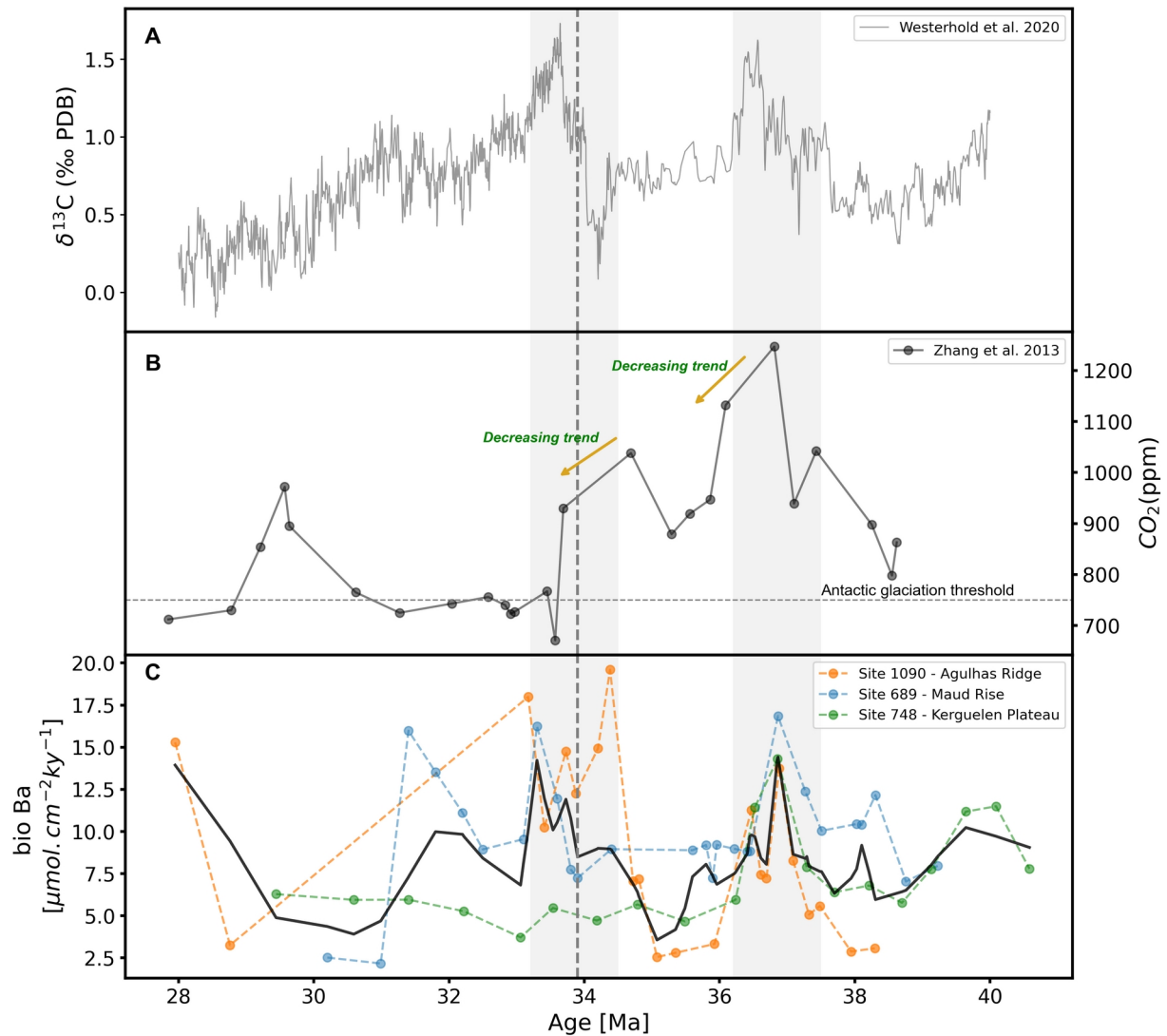
1114 **Figure 1: Schematic Antarctic Circumpolar Current (ACC) and Southern Ocean fronts as determined by Orsi et**
 1115 **al., 1995, named from north to south, STF: Subtropical front, SAF: Subantarctic Front; PF: Polar Front and**
 1116 **SACCF: Southern Antarctic Circumpolar Current Front, and sBdy: Southern Boundary front. Modern location**
 1117 **of ODP sites (1090, Agulhas Ridge; 689, Maud Rise and 748, Kerguelen Plateau) used for reconstructions in this**
 1118 **study. ODP = Ocean Drilling Program.**



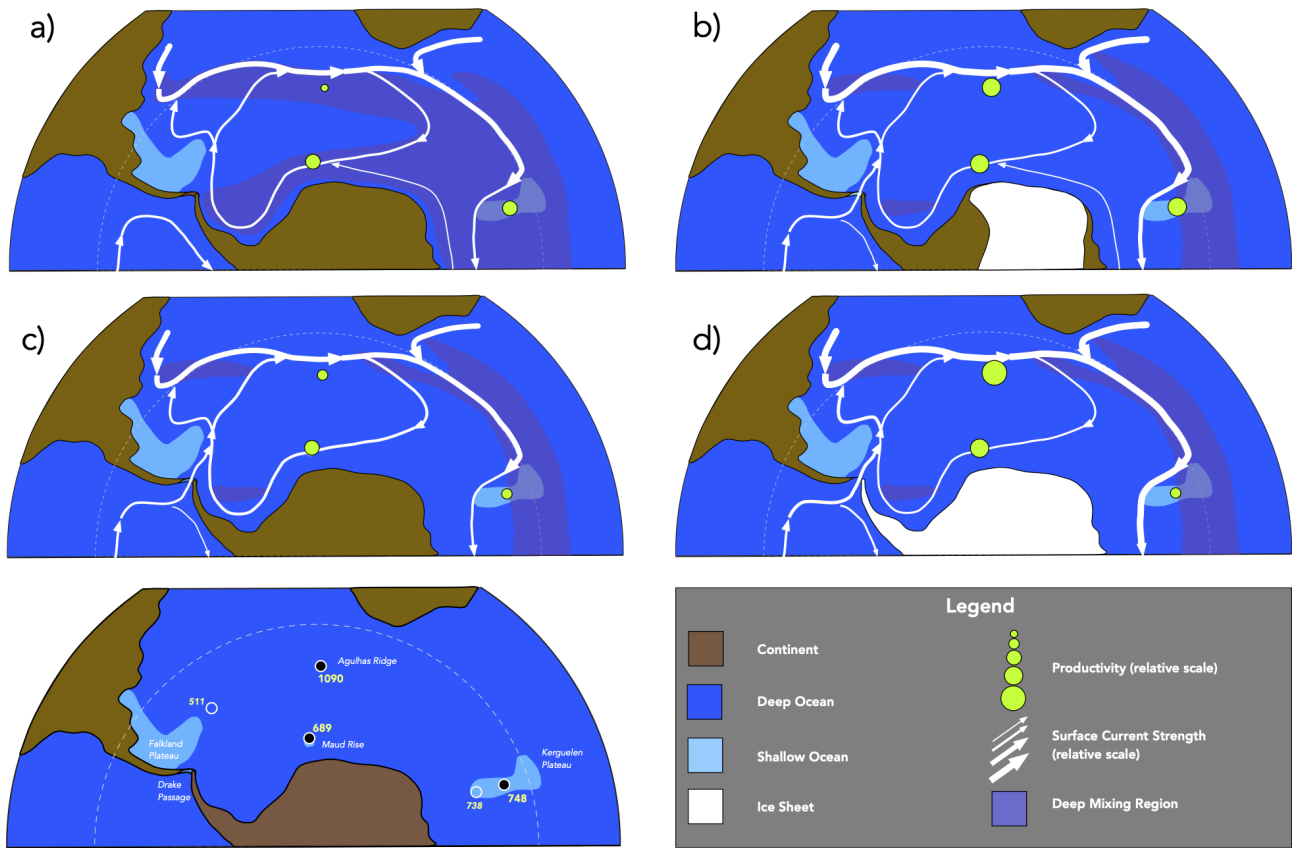
1119 **Figure 2: Paleoproductivity proxies vs Age (Ma) for Agulhas Ridge (ODP Site 1090, in orange), Maud Rise (ODP**
 1120 **Site 689, in blue) and Kerguelen Plateau (ODP Sites 748, 744, in green). Solid circles are new biogenic barium**
 1121 **accumulation rate (bio-Ba, $\mu\text{mol cm}^{-2} \text{kyr}^{-1}$) data of this study, open circles from prior literature (Agulhas Ridge**
 1122 **data from Anderson and Delaney, 2005; Maud Rise data from Diester-Haass and Faul 2019; Kerguelen Plateau**
 1123 **data from Faul et al., 2010). Site 1090 opal MAR data are from Diekmann et al., 2004. Site 689 BFAR data are**
 1124 **from Diester-Haass et al., 2019. Vertical bar identifies the E/O boundary (at ca 33.8 Ma). Shaded area**
 1125 **encompasses the late-Eocene productivity event.**



1126 **Figure 3: Multiproxy records from the late Eocene and early Oligocene. Global compilation of oxygen and**
 1127 **carbon stable isotopes (from Westerhold et al., 2020). New generated oxygen and carbon benthic foraminiferal**
 1128 **isotopes data (solid circles) and fine fraction (<45 μ m) (solid triangles), and previously published oxygen and**
 1129 **carbon stable isotopes (shaded circles, from Mackensen and Ehrmann, 1992; Diester-Haass and Zahn, 1996;**
 1130 **Bohaty et al., 2003) from Atlantic Southern Ocean (Maud Rise) ODP Site 689 (in blue) and Indian Southern**
 1131 **Ocean (Kerguelen Plateau) ODP Site 748 (in green). PDB is PeeDee Belemnite carbonate reference. Compilation**
 1132 **of ϵ Nd data obtained from fossil fish teeth for the Atlantic Sector of SO (Maud Rise, in blue, Site 689), and for**
 1133 **the Indian sector of SO (Kerguelen Plateau, in green, sites 738 and 748) (Scher and Martin, 2004, 2006; Scher et**
 1134 **al., 2014; Wright et al. 2018). Shaded area identifies E/O boundary at ca 33.8 Ma and productivity event at ca 37**
 1135 **Ma. Note inverted y-axis scales for oxygen and Nd isotopes.**



1136 **Figure 4: Comparison between (a) a global compilation of carbon stable isotopes (from Westerhold et al., 2020),**
 1137 **(b) alkenone-based atmospheric $p\text{CO}_2$ record (from Zhang et al., 2013) and (c) biogenic Barium (bio-Ba) export**
 1138 **productivity proxy (this study). Antarctic glaciation thresholds (approx. 750 ppm) (from climate model, DeConto**
 1139 **et al. 2008) is marked by a dashed line. Shaded areas encompass the late-Eocene and early-Oligocene high**
 1140 **productivity intervals.**



1141 **Figure 5: Interpretive scenario of paleoceanographic change in the late Eocene to earliest Oligocene Southern**
 1142 **Ocean. Base map, circulation patterns and extent of deep mixing regions largely after Toumoulin et al. (2020), ice**
 1143 **sheet extent at 38 Ma after models in Van Breendam (2022). Productivity values based on results of this study,**
 1144 **shown in relative scale. Note general trend towards higher productivity values, and within this, higher**
 1145 **productivity, focussed near proto-ACC, during intervals with inferred ice sheets.**